Original

Pemberton, P.; Nilsson, J.; Hieronymus, M.; Meier, H.E.M.:
Arctic Ocean Water Mass Transformation in S–T Coordinates.
In: Journal of Physical Oceanography. Vol. 45 (2015) 4, 1025 - 1050.
First published online by AMS: 01.04.2015

http://dx.doi.org/10.1175/JPO-D-14-0197.1

Arctic Ocean Water Mass Transformation in *S–T* Coordinates

PER PEMBERTON

Department of Meteorology, Stockholm University, Stockholm, and Oceanographic Research Unit, Swedish Meteorological and Hydrological Institute, Gothenburg, Sweden

JOHAN NILSSON

Department of Meteorology, Stockholm University, Stockholm, Sweden

MAGNUS HIERONYMUS

Institute for Coastal Research, Helmholtz Zentrum Geesthacht, Geesthacht, Germany

H. E. MARKUS MEIER

Department of Meteorology, Stockholm University, Stockholm, and Oceanographic Research Unit, Swedish Meteorological and Hydrological Institute, Norrköping, Sweden

(Manuscript received 23 September 2014, in final form 6 January 2015)

ABSTRACT

In this paper, water mass transformations in the Arctic Ocean are studied using a recently developed salinity–temperature (*S–T*) framework. The framework allows the water mass transformations to be succinctly quantified by computing the surface and internal diffusive fluxes in *S–T* coordinates. This study shows how the method can be applied to a specific oceanic region, in this case the Arctic Ocean, by including the advective exchange of water masses across the boundaries of the region. Based on a simulation with a global ocean circulation model, the authors examine the importance of various parameterized mixing processes and surface fluxes for the transformation of water across isohaline and isothermal surfaces in the Arctic Ocean. The model-based results reveal a broadly realistic Arctic Ocean where the inflowing Atlantic and Pacific waters are primarily cooled and freshened before exiting back to the North Atlantic. In the model, the water mass transformation in the *T* direction is primarily accomplished by the surface heat flux. However, the surface freshwater flux plays a minor role in the transformation of water toward lower salinities, which is mainly driven by a downgradient mixing of salt in the interior ocean. Near the freezing line, the seasonal melt and growth of sea ice influences the transformation pattern.

1. Introduction

The Arctic Ocean—the smallest of the world's oceans—provides a direct link between the Pacific and Atlantic Oceans. It is also a region of extreme climatic conditions leading to strong water mass modification of the inflowing water. The water masses of the Arctic Ocean are primarily of Atlantic origin, entering the Arctic Ocean both via the deeper Fram Strait and the shallower Barents Sea. During its northward transit the uppermost part (~200 m) of the Atlantic water experiences considerable water mass transformation via cooling and freshwater input subsequently forming cold, near-freezing polar surface and halocline waters (e.g., Rudels et al. 1996). The main sources of freshwater input that drive the haline transformation are river runoff and net precipitation. In addition, the low-saline Pacific water (which is slightly fresher than Atlantic water) acts to further freshen the uppermost water masses primarily on the North American side. Sea ice processes also contribute significantly to water mass transformation through the seasonal melt–freeze cycle, though the long-term net effect in the Arctic Ocean is a salinification because of the net growth and export of sea ice.

Denotes Open Access content.

Corresponding author address: Per Pemberton, Department of Meteorology, Stockholm University, SE-106 91 Stockholm, Sweden.
E-mail: per.pemberton@smhi.se

DOI: 10.1175/JPO-D-14-0197.1

Below the fresh and cold surface water a warmer ($T \sim 0$–$2°C$), saline, and less transformed variety of the Atlantic water resides at intermediate depths followed by cold and saline deep water in the abyss. The fresh and cold on top of warm and salty hydrographic structure is stable primarily because of the large freshwater input creating a sharp salinity gradient. In addition, the low temperatures reduce the thermal expansion coefficient, making the stratification less determined by the temperature gradient. This vertical structure, which effectively inhibits the heat stored in the Atlantic water to penetrate upward, is characteristic for the central Arctic and allows for a perennial ice cover to persist (e.g., Martinson and Steele 2001). Many studies of the Arctic Ocean have aimed to understand how this hydrographic structure is formed and maintained, and the present understanding is that both surface and internal (mixing) processes contribute (e.g., Aagaard et al. 1981; Steele et al. 1995; Rudels et al. 1996, 2004).

The water masses entering the Arctic Ocean eventually return to the North Atlantic Ocean (mainly through the Canadian Arctic Archipelago and the Fram Strait) and thus connect the Arctic Ocean to the Atlantic and global circulation. The flow of Atlantic water across the Arctic Mediterranean (the Arctic Ocean and the Nordic Seas) has by several authors been described as a double estuary (e.g., Stigebrandt 1985; Carmack 2007; Rudels 2010; Eldevik and Nilsen 2013) with Atlantic water transforming into either a denser water mass by cooling (negative estuary) or a lighter water mass by mixing with the freshwater input (positive estuary).

The distributions of the conservative ocean tracers temperature[1] T and salinity S have long been used in oceanography to identify water masses and their transformations (e.g., Worthington 1981). Through their relation to the density of seawater, the spatial distributions of these tracers contain information on the large-scale ocean circulation. In two pioneering papers, Walin (1977, 1982) demonstrated how water mass transformations, and aspects of the large-scale circulation, can be deduced from surface fluxes and interior mixing if conservation equations are formulated in tracer coordinates rather than in geographical coordinates. Focusing on estuarine circulations, Walin (1977) used salinity as the independent tracer coordinate and derived a relation between the volume flow across isohaline surfaces and the haline forcing due to surface fluxes and mixing. In a study with a global perspective, Walin (1982) formulated volume and heat conservation relations in temperature coordinates. Based on this framework, he provided an illuminating discussion of the ocean circulation viewed in temperature space using observationally based computations of the net ocean surface heat flux as a function of the sea surface temperature compiled by Andersson et al. (1982). Many investigators have subsequently used and extended the ideas of Walin (1977, 1982) to examine the transformation of water masses in the context of both observational- and model-based studies. These investigations include analyses of water mass transformation between density classes (Tziperman 1986; Speer and Tziperman 1992; Iudicone et al. 2008); transformations due to wind-induced near-surface mixing (Nilsson 1996); abyssal transformations due to geothermal heating (Emile-Geay and Madec 2008); studies of how mixed layer processes, eddies, and seasonality affect water mass transformations (Marshall 1997; Marshall et al. 1999); and methods to map water mass transformation and formation back to geographical locations (Brambilla et al. 2008; Maze et al. 2009).

In studies of the Arctic Ocean, the ideas of Walin have mainly been used to compute the net volume transport as a function of salinity across specific sections such as the Fram Strait and the Eurasian shelf edge (Rudels 1987, 1989; Nilsson et al. 2008). An advantage of representing the transport as a function of the salinity is that it provides direct information on the associated salt or freshwater transport. However, a description of the Arctic Ocean in terms of only salinity or temperature fails to capture some of the key water mass transformations in the region. A drawback with a description in temperature is that inflowing Atlantic and Pacific waters occupy similar temperature ranges, making geographical divisions necessary for distinguishing how these two inflows are modified in temperature. A salinity description is able to separate the inflowing waters reasonably well and has the advantage of giving the approximate density of the water masses. However, over a broad range of salinities there are counteracting transformation tendencies because of the freshwater input from rivers and the atmosphere and freshwater extraction from sea ice formation. Thus, a S–T description of Arctic water mass transformations would for many purposes be advantageous, and it has the virtue of better resolving sea ice–related transformations, occurring near the freezing line in S–T space.

In fact, a S–T framework for studying water mass transformations now exists in the literature, which is the result of the work of several researchers. Speer (1993) generalized the ideas of Walin to describe water mass transformations in both S and T coordinates. Specifically, he showed how knowledge of surface fluxes of heat and freshwater can be translated to a transformation vector that describes the strength and direction of the

[1] In this study temperature, denoted by T, refers to potential temperature as this is conserved by the numerical model used.

associated water mass transformation in S–T space. Speer (1993) used these ideas to study water mass transformations due to air–sea fluxes in the North Atlantic based on observations. Several researches have also decomposed the volume transports across specific geographical sections in T and S classes (e.g., Marsh et al. 2005; Rudels et al. 2008; Zika et al. 2013). By decomposing the volume transport into an ocean region in this way, aspects of the water mass transformations occurring in the region can be diagnosed. In an Arctic Ocean application, Rudels et al. (2008) used observations to decompose the volume transport through the Fram Strait into T and S classes.

Recently, Döös et al. (2012) and Zika et al. (2012) introduced a thermohaline streamfunction that describes the time-mean global ocean circulation in S–T coordinates. This streamfunction is related to Speer's vector-based description of water mass transformations. If the global ocean is in a steady state, then there is no net formation of water in any S–T class, implying that the vector field describing the net water mass transformation has to be nondivergent. Thus, in a steady state, the net transformation vector can be described by a streamfunction in S–T coordinates. In principle, the net transformation vector, and thus the thermohaline streamfunction, could be identical to zero. Interestingly, the global thermohaline streamfunction turns out to be nonzero, and it captures aspects of circulation patterns in geographical coordinates, including the interocean conveyor circulation (Döös et al. 2012). Groeskamp et al. (2014a) showed that the streamfunction introduced by Döös et al. (2012) and Zika et al. (2012), computed as a time mean of the instantaneous velocity components perpendicular to isothermal and isohaline surfaces, does not represent the total water mass transformation; there is an additional contribution arising from the seasonal movement of the isothermal and isohaline surfaces. Groeskamp et al. (2014a) denoted the total streamfunction due to the velocity field and the movements of the property surfaces, the diathermohaline function. Furthermore, they pointed out that this streamfunction is directly related to the thermohaline forcing due to surface fluxes and mixing (see also Groeskamp et al. 2014b).

Following the original ideas of Walin (1977, 1982), Hieronymus et al. (2014) formulated volume, heat, and salt budgets in S–T coordinates from which the relations between the volume flows across isothermal and isohaline surfaces and mixing, and surface fluxes are obtained. This provides a more formal derivation of the transformation vector due to Speer (1993) that now includes also the contribution from mixing in the ocean, illuminating the connection between the transformation vector and the diathermohaline streamfunction. Based on results from a global ocean circulation model, Hieronymus et al. (2014) used the generalized Walin formulae to investigate the role of surface fluxes and various parameterized mixing processes in creating the global diathermohaline streamfunction.

The framework developed by Hieronymus et al. (2014) is a useful tool for studying the processes responsible for the global water mass transformations. In addition, the framework can easily be extended to study water mass transformations in a specific oceanic region by including the volume, heat, and salt transports across the lateral boundaries of the region. In this context, the Arctic Ocean is an especially interesting region because of its characteristic settings where inflowing Atlantic and Pacific waters mix and strong water mass transformation occurs. Thus, the aim of the present study is to use and extend the results of Hieronymus et al. (2014) to examine water mass transformations in the Arctic Ocean. For this purpose, we analyze the results from a global ocean model, which allow us to identify the key processes in the model that transform the S–T characteristics of the Arctic Ocean water masses and the role of the heat and salt exchange with the North Pacific and North Atlantic.

The article is organized as follows: In section 2, we briefly present the theory of how water mass transformation can be studied in S–T coordinates. In section 3, we apply the method to the Arctic Ocean using a global ocean model. First, we analyze water mass transformations in salinity- or temperature-only coordinates; this is followed by analysis of transformations in S–T coordinates. Then the effect of model deficiencies is discussed in light of the simulated water mass transformations. In the final section, we summarize and conclude the main findings of our work. In addition, appendixes providing a more extensive explanation of the basic relations in the S–T framework are included.

2. The S–T framework

a. Basic equations

Here, we present the key equations that describe water mass transformations in the S–T coordinates. We closely follow the derivation of Hieronymus et al. (2014) and the details are presented in appendixes A, B, and C.

The water mass transformation relations are derived from the conservation of volume, heat, and salt in a subdomain of the ocean, the Arctic Ocean in the present application. Specifically, we consider the subregion $R(S, T, t)$, where the salinity is less than S and the temperature is less than T; $R(S, T, t)$ is in turn defined by the boundaries $A(S, T, t)$, $B(S, T, t)$, $I_S(S, T, t)$, and

$I_T(S, T, t)$, where the salinity is less than S and the temperature is less than T (see Fig. 1). The volume of this region is denoted $V(S, T, t)$, and the volume in the temperature and salinity range from T to $T + dT$ and S to $S + dS$ is (e.g., Worthington 1981)

$$v(S,T,t)dSdT,\ v(S,T,t) \equiv \frac{\partial^2 V}{\partial T \partial S}. \tag{1}$$

The conservation of volume for the subregion R can be written

$$\frac{\partial V}{\partial t} = -G_T - G_S - M - E. \tag{2}$$

Here, the right-hand sides are the volume transports across the boundaries of R; G_T and G_S are the volume flows across the isothermal and isohaline bounding surfaces, respectively; M is the boundary volume exchange flow with the rest of the ocean; and E is the net freshwater exchange through the sea surface. All flows are counted positive when leaving R, and G_T/G_S are the net volume fluxes across the isothermal/isohaline that can move themselves in space. Note that when we refer to the volume flows across the tracer surfaces, that is, the G_T/G_S, these flows should not be confused with Eulerian advection.

Walin (1977, 1982) realized that the net flow across isothermal/isohaline surfaces can be expressed in terms of the diffusive and surface fluxes of heat/salt independently of any time changes in V and the boundary exchange flow M. By using the conservation relations for salt and heat [see Hieronymus et al. (2014) and appendix B], one can show that

$$G_S = S\left(\frac{\partial E}{\partial S}\right) - \frac{\partial F_S}{\partial S}, \quad \text{and} \tag{3}$$

$$G_T = -\frac{1}{c}\frac{\partial Q}{\partial T} - \frac{1}{c}\frac{\partial F_T}{\partial T}. \tag{4}$$

Here, E and Q are the net fluxes out of the ocean of freshwater and heat, respectively, across the parts of the sea surface where the salinity is less than S and the temperature is less than T; c is the heat capacity per unit volume; and F_S and F_T are the diffusive salt and heat fluxes out of R, respectively (see Fig. 1). Note that G_T and G_S describe the transformation of water masses associated with changes in temperature and salinity.

b. The water mass transformation vector

Speer (1993) showed that water mass transformations can be represented by a two-dimensional vector that gives the strength and direction of the transformation in S–T coordinates. This vector can be defined as

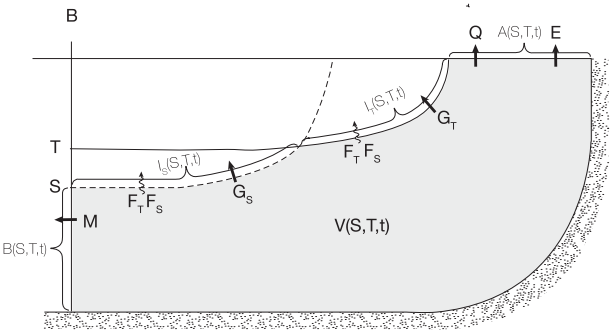

FIG. 1. Sketch showing the region $R(S, T, t)$, containing the volume $V(S, T, t)$; its boundaries $A(S, T, t)$, $I_T(S, T, t)$, $I_S(S, T, t)$, and $B(S, T, t)$; and the associate fluxes across each boundary. Note that the sketch is drawn to illustrate all the different surfaces and fluxes rather than represent a typical Arctic situation, which is more difficult to sketch in 2D. We refer to Fig. 10 for Arctic-like conditions of $V(S, T, t)$.

$$\mathbf{J} = \left(\frac{\partial G_S}{\partial T}, \frac{\partial G_T}{\partial S}\right). \tag{5}$$

The interpretation of $\mathbf{J}$ is as follows: $(\partial G_S/\partial T)dT$ gives the transformation of water toward higher salinities occurring at the salinity S in the temperature range T to $T + dT$, and $(\partial G_T/\partial S)dS$ gives the transformation of water toward higher temperatures at T in the salinity range S to $S + dS$. By using this and Eqs. (2) and (5), the rate of change of $v(T, S, t)$ can be written

$$\frac{\partial v}{\partial t} = -\nabla \cdot \mathbf{J} - m(S,T) - e(S,T), \tag{6}$$

where we have defined

$$\nabla \equiv \left(\frac{\partial}{\partial S}, \frac{\partial}{\partial T}\right), \quad m(S,T) \equiv \frac{\partial^2 M(S,T)}{\partial S \partial T},$$
$$e(S,T) \equiv \frac{\partial^2 E(S,T)}{\partial S \partial T}. \tag{7}$$

Here, a positive $m(S, T)dSdT$ and $e(S, T)dSdT$ yields a net outflow in the salinity range S to $S + dS$ and temperature range T to $T + dT$. Note that the source term related to the freshwater exchange is usually small and can therefore often be neglected. However, as will be shown the term due to advective exchange across the domain boundaries is highly significant in parts of the S–T space and can balance water mass formation because of the divergence or convergence of the transformation vector.

3. Application

a. Model setup

As our diagnostic tool to study water mass transformation in the Arctic Ocean, we use the coupled ocean

sea ice modeling framework NEMO version 3.2 (Madec 2008), including the Louvain-la-Neuve Sea Ice Model, version 2 (LIM2), sea ice model (Fichefet and Maqueda 1997). The model is run in a global configuration using the tripolar grid ORCA1 with a base resolution of 1°. Despite the relatively coarse resolution, the displaced poles over the Northern Hemisphere allow for a grid spacing of 30–60 km over the Arctic Ocean with the Canadian Arctic Archipelago represented by two gateways: the Barrow Strait and the Nares Strait. The vertical discretization uses 64 z levels starting at 6 m with a gradual increase to 204 m at the bottom; bottom topography is represented by the partial step approach. The model uses a linear free-surface formulation following Roullet and Madec (2000) and is thus only approximately salt and heat conserving.

In the model, unresolved mesoscale eddy effects are represented by isoneutral mixing (Redi 1982) and isoneutral advection (Gent and McWilliams 1990). Vertical mixing coefficients are solved using the TKE turbulent closure (Gaspar et al. 1990; Madec et al. 1998) with convection handled by locally enhanced background diffusivity. In addition, parameterizations for tidal mixing (Simmons et al. 2004) and unresolved bottom boundary flows (Beckmann and Döscher 1997) are used.

Air–sea fluxes for heat and freshwater are calculated using bulk formulations, and penetrative shortwave radiation uses a simple two-band scheme (Paulson and Simpson 1977). The sea ice–ocean fluxes assume a levitated ice model, and ice salt fluxes use a constant salinity of 6 g kg^{-1}. The sea surface salinity is restored toward the WOA05 value by way of a restoring freshwater flux. The time scale of this restoration is approximately 40 days. The model is forced by the DRAKKAR forcing set, version 4.3 (DFS4.3), which includes a blend of the ERA-40 reanalysis, ECMWF operational analysis, and satellite products (Brodeau et al. 2010).

b. Simulation

The simulation starts from an ocean at rest with temperature and salinity drawn from the *World Ocean Atlas 2005* (*WOA05*). Using a repeated 26-yr forcing cycle (years 1958–83), the model is run for 1500 yr to reach a near steady-state solution where the model drift is small. Then an additional cycle of 26 yr is run where the processes needed for calculating the water mass transformations are diagnosed from the model. The diagnostics are done online to fully resolve temporal variations, and the discretization of the fluxes follows Hieronymus et al. (2014), with the exception that the analysis is only done for the Arctic region (see Fig. 2). This means that additional terms for the boundary exchange flows $M(S, T)$ at the B sections—the different gateways to the Arctic Ocean—also have to be diagnosed. All calculations presented in this study are based on the time mean of the last 26-yr period.

FIG. 2. Map showing the model bathymetry with geographical locations mentioned in this study: Barrow Strait (BaS), Bering Strait (BeS), Barents Sea Opening (BSO), Fram Strait (FS), Nares Strait (NS), and St. Anna Trough (SAT). The black lines show the gateways to the Arctic Ocean where boundary exchange flows $M(S, T)$ have been calculated and together with the coast lines define the Arctic Ocean region used in this study.

Figure 3 shows the time-mean freshwater content (referenced to 34.8 g kg^{-1}) of the upper 254 m and the temperature maximum of the Atlantic layer. The model clearly captures the characteristic freshwater pool (Fig. 3a) over the Canada basin and a sharp gradient toward the Amundsen and Nansen basins. The inflow of warm Atlantic water across the Nansen basin is also evident (Fig. 3b); however, the downstream spreading along the basin boundary is not well simulated, making the Canadian side too cold. The inability to produce a realistic Arctic Ocean boundary current is a common problem among ocean circulation models (Holloway et al. 2007), and at the present model resolution, a well-simulated boundary current is not expected. However, the vertical water mass structure with a cold and fresh surface layer above a warm, salty Atlantic layer is generally well captured (Fig. 4). This makes the simulation suitable for studying the broad features of water mass transformations in the Arctic Ocean, which is the purpose of the present work.

The time-mean annual surface freshwater and heat fluxes are shown in Fig. 5. Over the Arctic region, the net

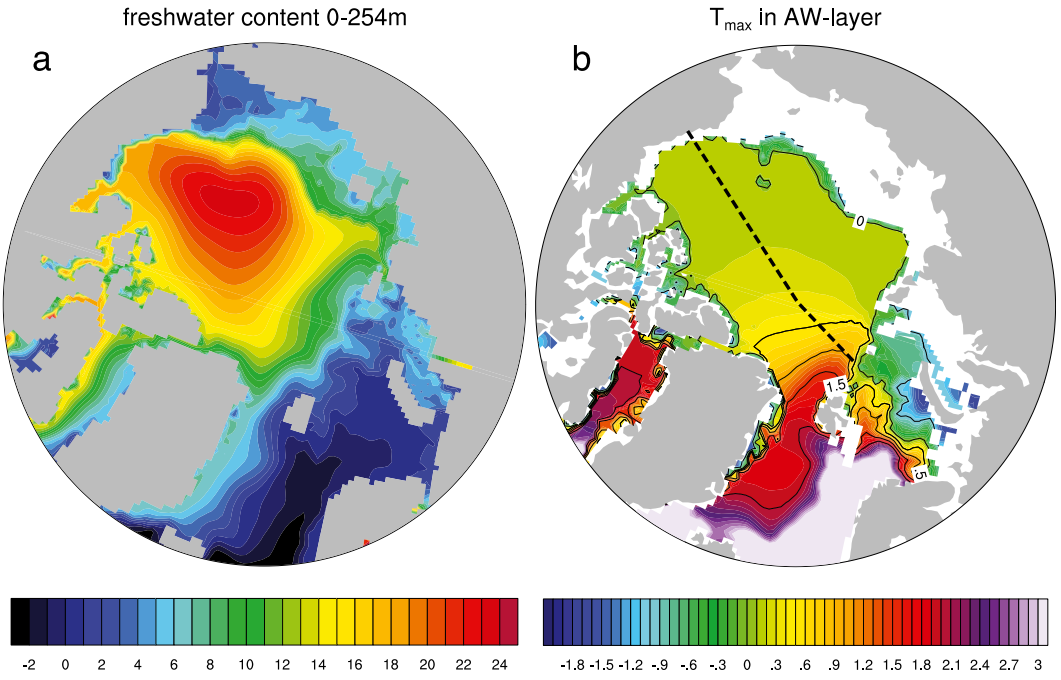

FIG. 3. (a) Time-mean freshwater content in m relative to a reference salinity of 34.8 g kg^{-1} integrated over the upper 254 m. (b) Potential temperature maximum (°C) in the Atlantic layer (200–1000 m). The dashed line shows the location of the transect in Fig. 4.

freshwater flux shows an input of freshwater in the proximity of the river mouths as well as over most parts of the Barents Sea, Kara Sea, East Siberian Sea, Chukchi Sea, and the Canada basin. A net loss of freshwater is seen along the Siberian coast in the Kara and Laptev Seas, around large islands in the Arctic, as well as over the Nansen and Amundsen basins and along the Alaskan coast in the Chukchi region. The net freshwater extraction along the coasts and islands is mainly because of the sea ice process (not shown). The dipole pattern across the central Arctic with a net input of freshwater over the Canada basin and extraction of freshwater over the Nansen and Amundsen basins is mainly because of the surface salinity restoring flux, which acts to maintain the sharp salinity front across the basins. The net heat flux over the Arctic region shows an overall heat loss with the strongest signals in the Barents Sea and west of Svalbard where the warm Atlantic water enters the Arctic as well as in the Chukchi Sea where warm Pacific water enters. A small net input of heat is seen in some regions that are seasonally ice free.

It should be noted that the present model has deficiencies in processes important for water mass transformations and uses the restoration of the sea surface salinity field. Thus, there are biases in the model-simulated hydrography and transformations, which will be further discussed in relation to observations in section 3g. However, to begin with, we describe and analyze the Arctic Ocean water mass transformations as they occur in the model.

c. *Water mass distribution of the Arctic Ocean*

Before considering transformations of water masses, we first discuss the composition of different water masses within the Arctic Ocean. The volumetric water mass distribution is given by $v(S, T, t)$ in Eq. (1), and similarly we define the surface area distribution as

$$a(S,T,t)dSdT,\ a(S,T,t) \equiv \frac{\partial^2 A}{\partial T \partial S}. \tag{8}$$

Figure 6 shows the time-mean volumetric and surface area distributions for the Arctic Ocean. Many different water classes are usually identified for surface and subsurface waters of the Arctic Ocean [see, e.g., Rudels (2009), Aksenov et al. (2010), and references therein for a full presentation of the different classes]. As the model in this study has a relatively coarse resolution, we only use the most basic definition of water masses characterizing the broad-scale features of the region. Here, we distinguish between the following:

1) The Polar Surface Water, which comprises the fresh and cold polar mixed layer and the halocline. Here, we define the polar mixed layer as the water mass where $S < 30.5$ g kg^{-1} and the halocline as the water

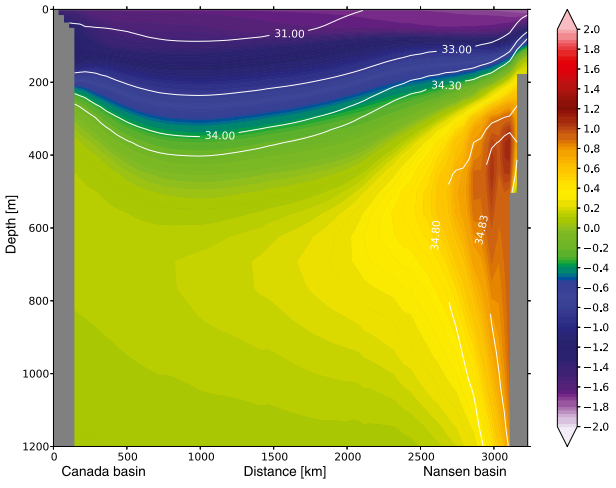

FIG. 4. Arctic-wide time-mean potential temperature (°C) along the transect in Fig. 3b (filled contours) and salinity ($g\,kg^{-1}$) for a selected number of isohalines marking the surface, halocline, and Atlantic waters (white lines).

mass where $30.5 < S < 34.3\,g\,kg^{-1}$ and $T \in [T_f, 0]$°C, where T_f is the freezing temperature of seawater.

2) The Atlantic water, which is usually defined as the subsurface layer below and above the $T = 0$°C isotherm and $S \in [34.8, 35]\,g\,kg^{-1}$.
3) The Pacific water, which has a large temperature range centered around a narrow salinity range; here, we use $T \in [0, 6]$°C and $S \in [30.5, 32.5]\,g\,kg^{-1}$.
4) The Polar Deep Water, which is the cold and salty water mass with $T < 0$°C and $S \in [34.5, 35]\,g\,kg^{-1}$ that resides under the Atlantic layer (see inset in Fig. 6a). Note that we do not distinguish between Polar Intermediate and Deep Water in this study, as is usually done (e.g., Aksenov et al. 2010; Rudels 2009).

In Fig. 6, the $v(S, T)$ and $a(S, T)$ over the Arctic Ocean are shown for two different climatologies, *WOA05* and the Polar Science Center Hydrographic Climatology 3.0 (PHC) (Steele et al. 2001), as well as from the simulation. Note that the climatological $v(S, T)$ and $a(S, T)$ are calculated from monthly data with a much sparser geographical sampling, while the simulated case is calculated online at every time step. This leads to a smoother and more even distribution for the latter. It is seen that the simulated $v(S, T)$ agrees reasonably well with both climatologies, capturing the basic water masses in the Arctic Ocean. However, the model has some shortcomings. The Atlantic water is somewhat too cold and fresh, and the halocline is too warm. The halocline region and upper part of the Atlantic water layer does not have the characteristic curve-shaped region in $S \in [31.5, 34.5]\,g\,kg^{-1}$. In addition, the Polar Deep Water is also too warm and fresh compared to both climatologies. Compared to the observations, the simulated $a(S, T)$, which shows regions where surface processes are active, is much more evenly distributed, presumably because it better samples the seasonal cycle. The bulk of the polar mixed layer is also spread over a wider salinity range compared to the climatologies that are centered around $S \in [30, 32]\,g\,kg^{-1}$. Notably, the PHC $a(S, T)$ shows a shift toward more salty surface waters close to the freezing line compared to *WOA05*. We also note that both the simulation and *WOA05* climatology have supercooled water. For the simulation this is presumably an artifact due to the nonmonotonic advection scheme and the surface salinity restoring, whereas for the climatology the problem may arise from spatial and temporal extrapolation.

d. *Exchange and transformation in temperature- or salinity-only coordinates*

It is illuminating to first study the water mass exchange and transformation in a salinity- or temperature-only coordinate framework: the 1D frameworks of Walin (1977, 1982). How to recover the 1D frameworks from the S–T framework is described in appendix C. In what follows, we will discuss the volume exchange between the Arctic Ocean and the exterior as well as the water mass transformation within the Arctic, as described by the 1D frameworks. The fluxes are diagnosed from our model simulation and represent a steady-state situation.

By setting $T = T_{\max}$, where $T_{\max}$ is a temperature above the range found in the Arctic Ocean, the temperature dependence drops out of the conservation relations, and the Walin (1977) S-coordinate description is obtained (see appendix C). Specifically, the cross-isothermal volume flow G_T is zero since the domain no longer has an isothermal boundary part. Thus, the steady-state volume budget reduces to

$$G_S(S) + M(S) + E(S) = 0, \tag{9}$$

where $G_S(S)$ is a short-hand notation for $G(S, T_{\max})$ and so forth. Similarly, by setting $S = S_{\max}$, where $S_{\max}$ is salinity above the range found in the Arctic Ocean, the salinity dependence drops out of the conservation relations, and the Walin (1982) T-coordinate description is obtained. In this case, the steady-state volume budget reduces to

$$G_T(T) + M(T) + E(T) = 0, \tag{10}$$

where again $G_T(T)$ is a short-hand notation for $G_T(S_{\max}, T)$ and so forth.

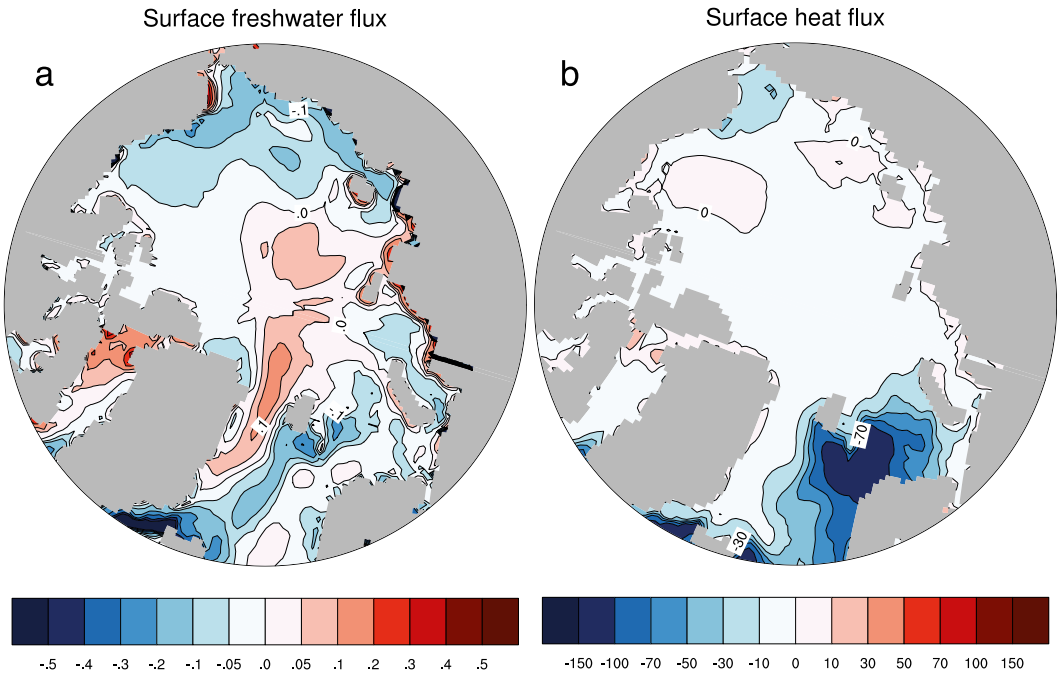

FIG. 5. (a) Time-mean net freshwater flux (mSv) counted positive when leaving the ocean. The freshwater flux includes the sea ice salt flux that has been converted into an equivalent water flux by scaling with the local salinity. (b) Net downward heat flux (W m^{-2}).

In the S-coordinate description, the boundary exchange flow through the interior boundaries and the freshwater input through the sea surface are in a small salinity range S to $S + dS$ given by $m(S)dS$ and $e(S)dS$, respectively, where we have defined

$$m(S) \equiv \frac{\partial M(S)}{\partial S}, \quad e(S) \equiv \frac{\partial E(S)}{\partial S}. \tag{11}$$

Analogously for the T-coordinate description, we can define the boundary exchange and freshwater input $m(T)dT$ and $e(T)dT$ in a small temperature range dT. By inspecting the gradients of M and E, we can thus interpret if there is a net inflow (negative gradient) or outflow (positive gradient) in a certain salinity/temperature range. Here, the sign convention of M and E in Fig. 1 is assumed, meaning that they are positive when there is a flow out of the Arctic Ocean.

Figure 7 shows the net total volume exchange $M + E$, consisting of the boundary exchange flow M between the Arctic, North Atlantic, and Pacific Oceans as well as the freshwater exchange E in salinity and temperature coordinates. It is readily seen that the total volume exchange is dominated by M both in S and T coordinates, as expected. Note that since a steady state is considered, the flow that crosses the isohaline surfaces G_S (or isothermal surfaces G_T) equals $-M - E$. Thus, Fig. 7 shows that the haline water mass transformation is dominantly directed toward lower salinities. However, a weak transformation toward higher salinities occurs for salinities less than about 31. Here, $G_S \approx -E$, that is, the cross-isohaline flow balances the net freshwater input. The cross-isothermal volume flow G_T is also dominantly negative, indicating transformation toward lower temperatures, with the exception of a weak transformation toward higher temperatures near the freezing point.

In salinity coordinates (Fig. 7a), there is an inflow both at low salinities, primarily owing to a net freshwater input from river runoff (from the E term), and at high salinities, owing to an input of Atlantic water. In between there is a more complex signal with outflow at lower salinities interrupted by a net inflow at the range of Pacific water followed by outflow at intermediate salinities. The total volume exchange in salinity coordinates shows the estuarine character of the Arctic Ocean, where inflowing warm and salty Atlantic water is transformed by the surface processes as well as Pacific water input to eventually exit the Arctic back to the North Atlantic as Polar Surface Water. The features of the $M(S)$ exchange in the present model are similar to those found by Pemberton et al. (2014) in a regional coupled sea ice–ocean model.

In temperature coordinates it is seen (Fig. 7b) that the total and boundary exchange $M(T)$ is mainly directed out of the Arctic Ocean for $T < 1$°C and into the Arctic for higher temperatures. The freshwater exchange $E(T)$

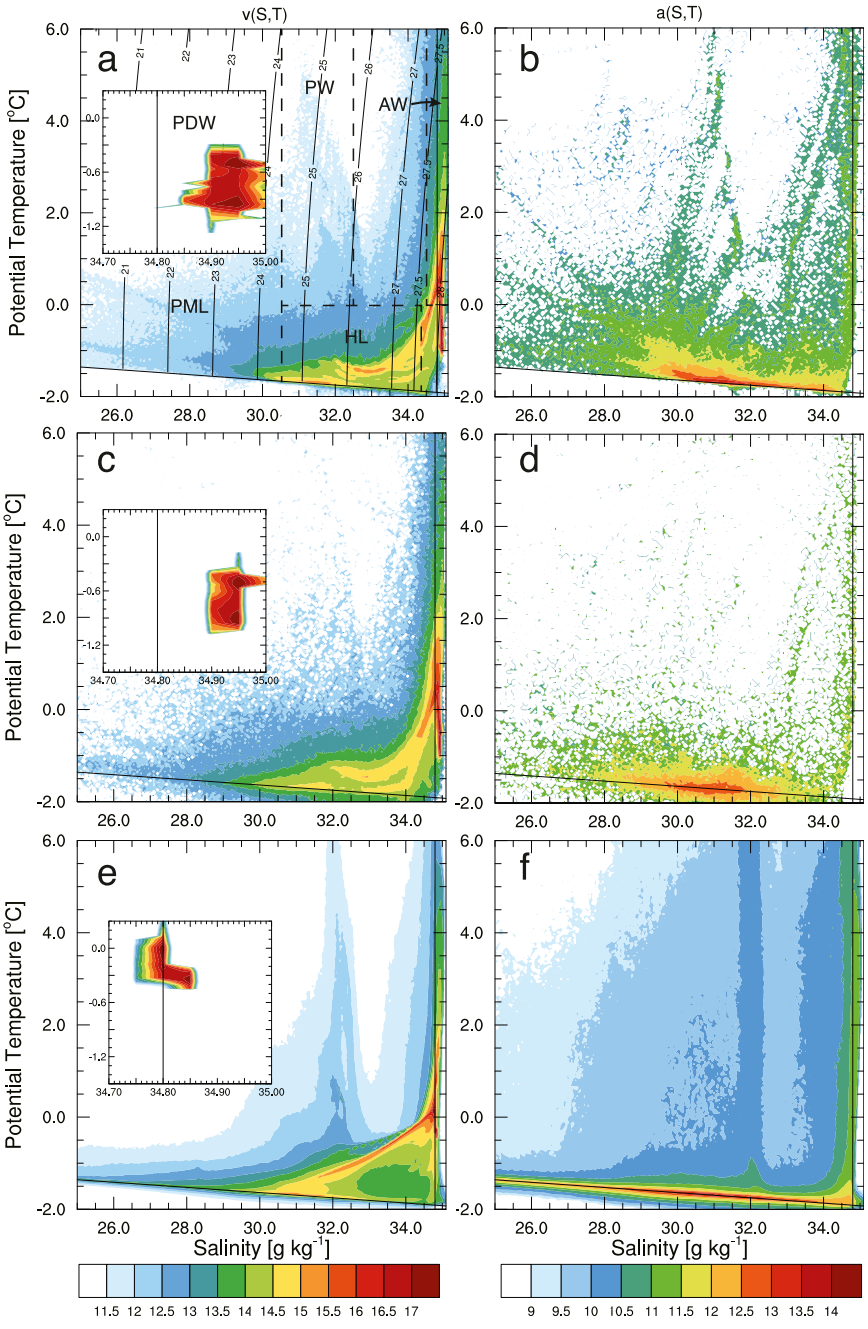

FIG. 6. The time-mean volumetric S–T distribution $v(S, T)$ {log10 [m^3 (°C S)$^{-1}$]} and the surface S–T distribution $a(S, T)$ {log10 [m^2 (°C S)$^{-1}$]} calculated over the Arctic Ocean region, defined in Fig. 3. The left column shows $v(S, T)$ for (a) PHC, (c) *WOA05*, and (e) model simulation. The right column shows $a(S, T)$ for (b) PHC, (d) *WOA05*, and (f) model simulation. For the distributions based on the two climatologies, monthly values are used, and for the model distributions, calculations are done at the model time step. In (a), a selected number of σ_0 isopycnals (thin black) as well as the Arctic water masses, polar mixed layer (PML), halocline layer (HL), Pacific water (PW), and Atlantic water (AW), are marked out (black dashed boundaries). The insets in (a),(c), and (e) show the $v(S, T)$ below 1000 m, roughly corresponding to the Polar Deep Water (PDW).

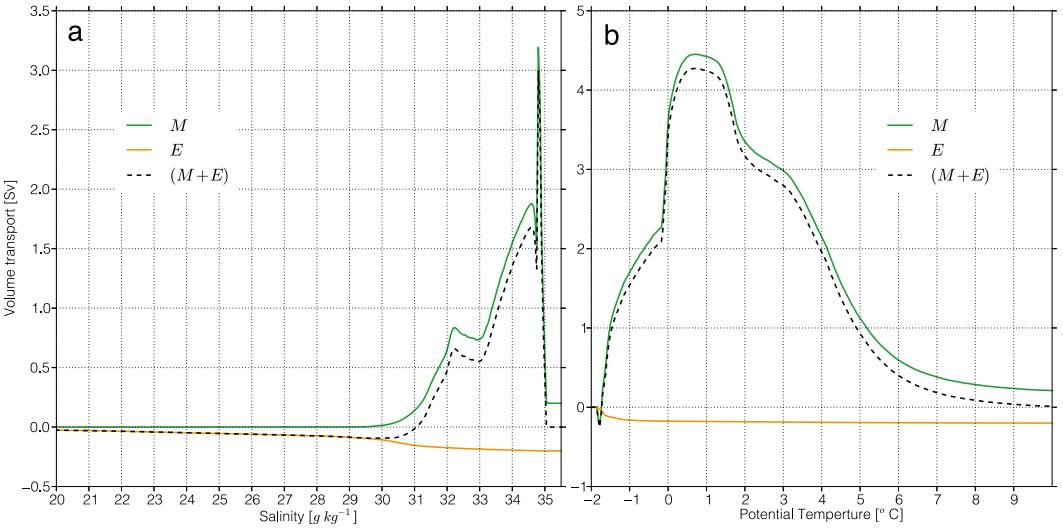

FIG. 7. Cumulative volume exchange M across the interior boundaries B and the net freshwater exchange E, both in Sv for (a) salinity less than S and (b) temperature less than T. The fluxes are calculated across the interior boundaries and sea surface area defined in Fig. 2.

shows an input predominantly at the very low temperatures, which is expected as most of the sea surface in the Arctic Ocean is near the freezing temperature (see, e.g., Fig. 6f).

By using the relation between G_S and surface fluxes and mixing [Eq. (3)], the steady-state volume budget in salinity coordinates [Eq. (9)] can be written as

$$S\frac{\partial E(S)}{\partial S} - \frac{\partial F_S(S)}{\partial S} + M(S) + E(S) = 0, \qquad (12)$$

and the salt budget can be rewritten as (see appendix C)

$$F_S(S) = SE(S) + \int_0^S M(S')\,dS'. \qquad (13)$$

In Eq. (12), the first two terms represent the cross-isohaline volume transport $G_S(S)$, which is positive if there is a transformation toward higher salinities and should balance the boundary volume exchange $M(S)$ and freshwater exchange $E(S)$. Equation (13) shows that in a steady state, the diffusive salt flux across the isohaline S is balancing the virtual salt flux $SE(S)$ and the boundary salt flux $\int_0^S M(S')\,dS'$ across the surface B, where salinity is less than S; note that the sum of the two terms on the right-hand side equals the net advective export of salt across the isohaline surface I_S and the lateral boundary surface B. To investigate different interior mixing processes, we decompose the diffusive fluxes F_S and F_T into separate components representing vertical and isoneutral mixing. Note that we have also investigated all other explicitly represented processes (including convection and the bottom boundary layer parameterization) in the model that contribute to material changes of temperature or salinity. However, the transformations due to these additional processes were found to be very small compared to the ones associated with vertical and isoneutral mixing and are not discussed further here.

From the cumulative salt balance it is seen (Figs. 8a,b) that the surface processes SE yield a flow toward lower salinities for $S < 31\,\mathrm{g\,kg^{-1}}$ and toward higher salinities in the range $S \in [31, 34]\,\mathrm{g\,kg^{-1}}$, while for $S > 34\,\mathrm{g\,kg^{-1}}$ they again yield a flow toward lower salinities. This acts to increase the salinity range in the Arctic Ocean over the interval where most of the polar mixed layer and halocline water reside, while a freshening is implied for salinities just below the Atlantic water range. The diffusive fluxes yield a flow toward higher salinities for $S < 31\,\mathrm{g\,kg^{-1}}$ and toward lower salinities above, thus acting to reduce the salinity range in the Arctic Ocean. The cumulative boundary salt exchange flux shows an export in the range $S \in [31, 35.5]\,\mathrm{g\,kg^{-1}}$.

Figure 8b clearly shows that the volume balance of Eq. (12) has two different regimes. At low salinities $S < 31\,\mathrm{g\,kg^{-1}}$, the balance is between the surface term $S\partial E(S)/\partial S$ and the diffusive terms $-\partial F_S(S)/\partial S$ as $M(S) = 0$ and $E(S)$ is small. Thus, here there is a strong cancellation between salinification due to mixing and dilution due to freshwater input, which results in only a small net transformation $[G_S(S) \approx -E(S)]$ directed toward higher salinities. This situation is expected to primarily occur on the shelf, where salinity is low and there is no direct advective exchange with the Atlantic and Pacific Oceans. At high salinities, the

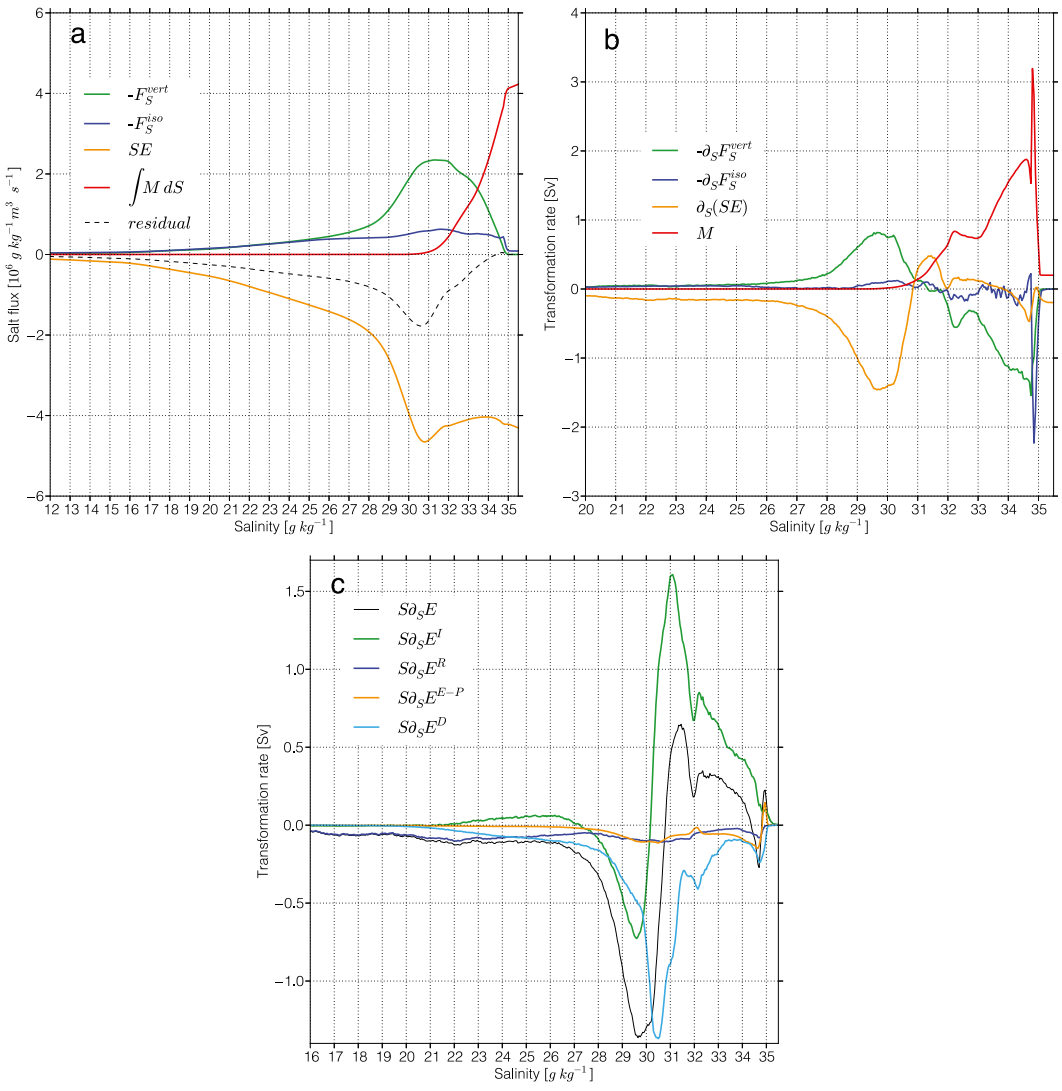

FIG. 8. The process-by-process balance for the salinity coordinate case: (a) the cumulative salt budget (10^6 g kg^{-1} m^3 s^{-1}), (b) the water mass transformation balance (Sv), and (c) the surface term $S\partial E/\partial S$ (Sv). In (c), the different parts of $S\partial E/\partial S$ are the total (thin black), net sea ice formation (green), runoff (dark blue), net evaporation (yellow), and surface salinity restoring (light blue).

balance is between the transformation due to mixing $-\partial F_S(S)/\partial S$ and the advective exchange $M(S)$. This applies over the salinity range where most polar mixed layer and halocline waters are exported out of the Arctic. In addition, it is seen that the vertical mixing generally contributes more than isoneutral mixing to the $\partial F_S(S)/\partial S$, except for $S \in [34.5, 35]$ g kg^{-1}, where there is a peak in the isoneutral mixing contribution.

To further examine the role of the different freshwater sources and sinks in the Arctic Ocean, we have decomposed the $S\partial E(S)/\partial S$ into different components of the surface freshwater balance. The results are presented in Fig. 8c, which shows the runoff, net sea ice formation, net evaporation, and surface salinity restoring components. It can be seen that the runoff and sea surface restoring act to force a transformation toward lower salinities, that is, act to freshen the Arctic Ocean. The restoring term is quite large and partly cancels the effect of the net sea ice formation. Net evaporation also mostly acts to freshen the Arctic Ocean except for $S > 34.8$ g kg^{-1}. The main process acting to salinify the Arctic Ocean is the net sea ice formation. For $S < 27$ and $S > 30$ g kg^{-1}, the net sea ice formation yields a transport toward higher salinities because of the net ice growth. In between ($27 < S < 30$ g kg^{-1}) the sea ice processes instead yield a freshening, indicating a net sea ice melt in this salinity interval.

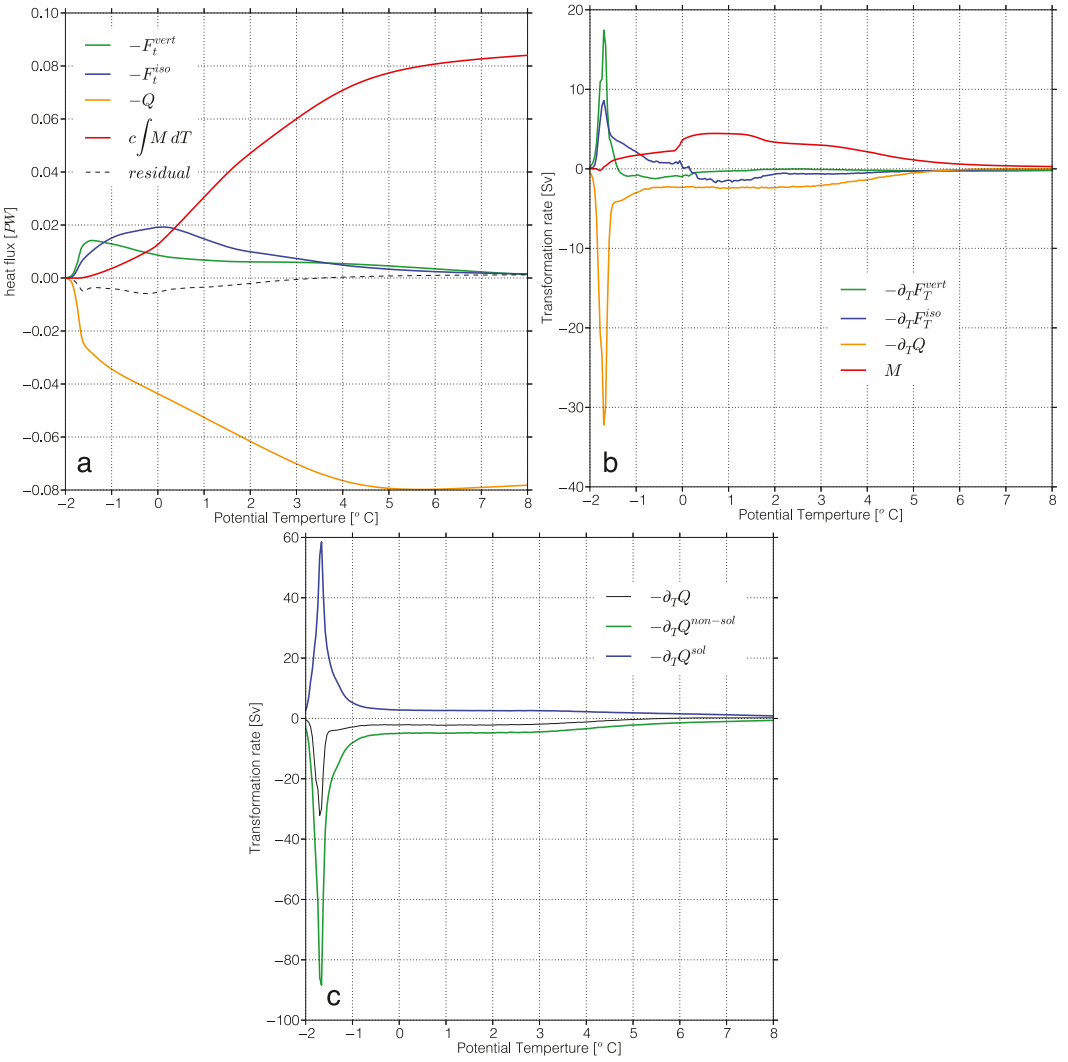

FIG. 9. The process-by-process balance for the temperature coordinate case: (a) the cumulative heat budget (PW), (b) the water mass transformation balance (Sv), and (c) the surface term $c^{-1}\partial Q/\partial T$ (thin black) (Sv) decomposed into solar (green) and nonsolar, including sensible heat flux, latent heat flux, and longwave radiation (blue) flux components.

By using a similar procedure as when deriving Eq. (12), the steady-state volume budget in the T-coordinate representation [Eq. (10)] can be rewritten as

$$-\frac{1}{c}\frac{\partial Q(T)}{\partial T}-\frac{1}{c}\frac{\partial F_T(T)}{\partial T}+M(T)+E(T)=0, \quad (14)$$

and the cumulative heat budget can be written as

$$F_T(T)=-Q(T)+c\int_{T_{\min}}^{T}E(T')\,dT'+c\int_{T_{\min}}^{T}M(T')\,dT'. \quad (15)$$

Similar to Eq. (12), Eq. (14) expresses the volume balance for a region $R(S_{\max}, T)$ where the temperature is less than T, and the first two terms represent the cross-isothermal volume transport $G_T(T)$, which is positive if there is a transformation toward higher temperatures. Furthermore, Eq. (15) shows that the diffusive heat flux across the isothermal surface T is balancing the net surface heat loss over the part of the ocean surface, where the temperature is less than T, and the advective heat flux $c\int_{T_{\min}}^{T}M(T')\,dT'$ across the part of the interior boundary B, where the temperature is less than T. Note that the second term on the right-hand side, which is the heat carried by the net freshwater exchange, is incorporated into the $Q(T)$ term in our analysis below.

Figures 9a and 9b show the cumulative heat balance in temperature coordinates. Here, the surface heat exchange

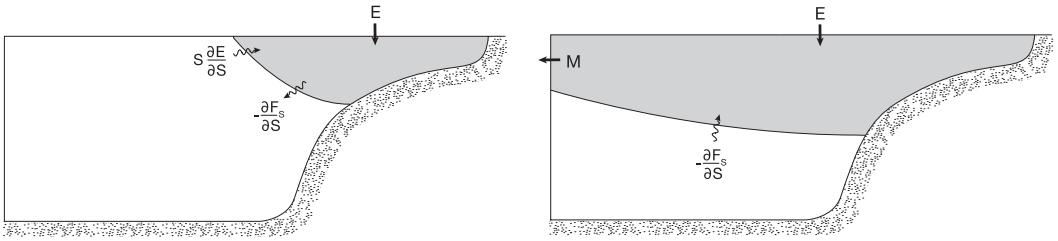

FIG. 10. A sketch showing the dominating balance of Eq. (12) in the Arctic Ocean in the case of (left) low salinity and (right) high salinity. Note that the E term is usually small.

yields a transformation toward lower temperatures due to a net heat loss for $T < 6$°C, where most of the Arctic Ocean water mass can be found (see Fig. 6f). For low temperatures the diffusive cumulative heat fluxes yield a transformation toward higher temperatures and for high temperatures a flow toward lower temperature. Thus, similar to the cross-isohaline diffusive fluxes, the cross-isothermal diffusive fluxes induce a transformation that acts to decrease the temperature range. The cumulative advective heat exchange in temperature coordinates represents an overall import of heat occurring over a wide range of temperatures.

The volume balance of Eq. (14) in temperature coordinates is shown in Fig. 9b. It is seen that the surface heat flux term $-c^{-1}\partial Q(T)/\partial T$ is negative with a peak close to the freezing point, yielding a flow toward lower temperatures. The surface heat flux is further decomposed into solar (shortwave radiation) and nonsolar (sensible heat flux, latent heat flux, and longwave radiation) components (Fig. 9c), and as expected the solar component acts to heat up the Arctic, while the nonsolar component leads to a cooling. The vertical and isoneutral diffusive fluxes both yield a flow toward higher temperatures, peaking close to the freezing point, and flow toward lower temperatures over a wide range of higher temperatures (Fig. 9b). In the higher temperature range it is the isoneutral mixing together with the surface heat flux that dominates the transformation toward lower temperatures. Similar to the salinity coordinate case, there is a range where the balance is only between the surface heat flux term and the diffusive fluxes and a range where the balance is between the advective exchange term $M(T)$ and the diffusive as well as the surface heat flux term.

Figures 8a and 9a both show that the residuals are typically smaller than the most dominating terms in the cumulative salt and heat equations; however, the budgets are not fully closed. The $\partial V/\partial t$ term is found to be small (not shown), and the residuals are likely a result of the linear free-surface formulation and the sea ice salt flux formulations that can introduce errors in the heat and particularly salt budgets [see, e.g., Roullet and Madec (2000) and Tartinville et al. (2001) for a further discussion on these issues].

Figure 10 illustrates two limiting situations for Arctic Ocean water mass transformations in salinity coordinates. For low salinities, the balance is primarily between opposing transformations because of the changes in freshwater input $S\partial E(S)/\partial S$ and the changes in the diffusive salt flux because of $\partial F(S)/\partial S$,

TABLE 1. Mean volume transports (Sv) for the different gateways to the Arctic Ocean, calculated by summing the $m(S, T)dSdT$ distributions. We have also included a number of recent observational estimates from the literature, most of which are compiled in Beszczynska-Möller et al. (2012). Note that the observational estimates are given within the parentheses.

Location	Inflow	Outflow	Net
Fram Strait	1.1 (3.0, 4.0)[a]	−2.8 (−4.5, −6.0)[b]	−1.7 (−1.6 ±3.9)[c]
	(3.8 ±1.7)[c] (6.6)[d]	(−5.4 ±2.1)[c] (−8.6)[d]	(−2.0 ±2.7)[a]
Barents Sea Opening	2.8 (4.5 ±0.8)[c] (3.2) [e]	−0.1 (−0.9 ±0.6)[c] (−0.9)[e]	2.7 (3.6 ±1.1)[c] (2.0)[e]
Bering Strait	1.3		1.3 (0.8 ±0.2)[f]
Barrow Strait		−0.6	−0.6 (−0.7)[g]
Nares Strait		−1.9	−1.9 (−0.57)[h] (−0.9)[i]
All	5.2	−5.4	−0.2 (−0.15 ±4.1)[c]

[a] Schauer et al. (2008), [b] de Steur et al. (2009), [c] Tsubouchi et al. (2012)
[d] Beszczynska-Möller et al. (2012), [e] Smedsrud et al. (2010), [f] Woodgate et al. (2005)
[g] Prinsenberg et al. (2009), [h] Münchow and Melling (2008), [i] Münchow et al. (2007)

TABLE 2. Transport-weighted mean inflow and outflow temperatures and salinities for the different gateways to the Arctic Ocean. Note that the weighting is done with the $m(S, T)dSdT$ distributions.

Location	Inflow		Outflow	
	T (°C)	S (g kg^{-1})	T (°C)	S (g kg^{-1})
Fram Strait	1.6	34.9	−0.3	34.4
Barents Sea Opening	4.6	34.9	0.2	34.5
Bering Strait	0.3	32.5	—	—
Barrow Strait	—	—	−1.5	31.5
Nares Strait	—	—	−1.1	32.9
All	2.9	34.3	−0.7	33.6

as the boundary exchange term vanishes [$M(S) = 0$] and the freshwater input $E(S)$ is small. Here, the dilution due to the freshwater input is balanced by a diffusive downgradient salt flux, yielding the salt budget $F_S(S) = SE(S)$. In the case of high salinity, on the other hand, the balance is instead between the boundary exchange term $M(S)$ and a cross-isohaline volume flow toward lower salinity that is accomplished essentially through the mixing-related term $\partial F(S)/\partial S$, with weak direct influence of surface freshwater fluxes.

e. *Inflow distributions in S–T coordinates*

The Arctic Ocean water mass transformations viewed in salinity or temperature coordinates yield a simple leading-order picture. In temperature space, the advective exchange term $M(T)$ shows how warm, inflowing waters are essentially transformed to cold, outflowing waters. In salinity coordinates, $M(S)$ yields a similar picture; saline inflowing waters are chiefly transformed toward less saline outflowing waters. Looking more closely at $M(S)$, one can identify a Bering Strait inflow signature at lower salinity and Barents Sea and Fram Strait inflow signatures. However, some features of the water mass transformations tend to be obscured when only using T or S frameworks, and here the S–T framework can provide more detailed information about the transformations. One reason to use a S–T framework is that the Atlantic water inflows and cold dense outflows are not well separated in salinity, and in temperature the Atlantic and Pacific inflows occupy similar temperature ranges. Further, a S–T framework should better resolve surface flux–induced transformations, which in the Arctic Ocean tend to occur in a small range of S–T values near the freezing line.

Thus, we now proceed to analyze the Arctic Ocean water mass transformations in S–T coordinates. To begin with, we focus on the boundary exchange distributions $m(S, T)$ at the different gateways to the Arctic Ocean, which we here refer to as inflow distributions. We have also calculated the mean volume transports (Table 1) as well as the transport-weighted mean salinities and temperature (Table 2) at the different gateways, using the $m(S, T)dSdT$ distributions as weights.

Figure 11a clearly shows the signature of water mass transformations occurring in the Arctic Ocean. Two distinct water types flow into the Arctic: the warm and salty Atlantic water and the slightly fresher Pacific water. This leads to a transport-weighted mean of $T = 2.9$°C and $S = 34.3\,\mathrm{g\,kg^{-1}}$ for the inflowing waters. These source waters are then generally cooled and freshened in the Arctic Ocean, leading to a mean outflow characterized by $T = -0.7$°C and $S = 33.6\,\mathrm{g\,kg^{-1}}$.

We also note from Table 2 that the volume transport in the model is generally in good agreement with recent observational estimates compiled in Beszczynska-Möller et al. (2012) as well as with the inverse model study of Tsubouchi et al. (2012). However, the simulated Fram Strait inflow of 1.1 Sverdrups (Sv; 1 Sv $\equiv 10^6\,\mathrm{m^3\,s^{-1}}$) is lower than the observed estimate of 3.0–6.6 Sv by Schauer et al. (2008) and Beszczynska-Möller et al. (2012). Likewise, the simulated Fram Strait outflow of 2.8 Sv is lower than their observational estimates of 4.5–8.6 Sv. This gives a simulated Fram Strait net volume transport of −1.7 Sv that is within the observed ranges of -1.6 ± 3.9 by Tsubouchi et al. (2012) and the -2.0 ± 2.7 Sv by Schauer et al. (2008). The simulated Barents Sea Opening net inflow of 2.7 Sv is also slightly higher than the 2.0 Sv estimated from observations by Smedsrud et al. (2010). In addition, it is also seen that the simulated inflow of 1.3 Sv through the Bering Strait is higher than the observed 0.8 ± 0.2 Sv estimated by Woodgate et al. (2005). Across the Canadian Arctic Archipelago the simulated net outflow of 0.6 Sv through the Barrow Strait is in line with the 0.7 Sv from observations by Prinsenberg et al. (2009). While at the Nares Strait the simulated outflow of 1.9 Sv is much higher in the model compared to the 0.6–0.9 Sv estimated from observations by Münchow et al. (2007) and Münchow and Melling (2008). It should be noted, however, that the model only has two gateways (the Barrow and Nares Straits) in the Canadian Arctic Archipelago, whereas observational volume budgets (e.g., Beszczynska-Möller et al. 2012) usually also include Cardigan Strait and Hell Gate with an additional volume transport of −0.3 Sv (Melling et al. 2008).

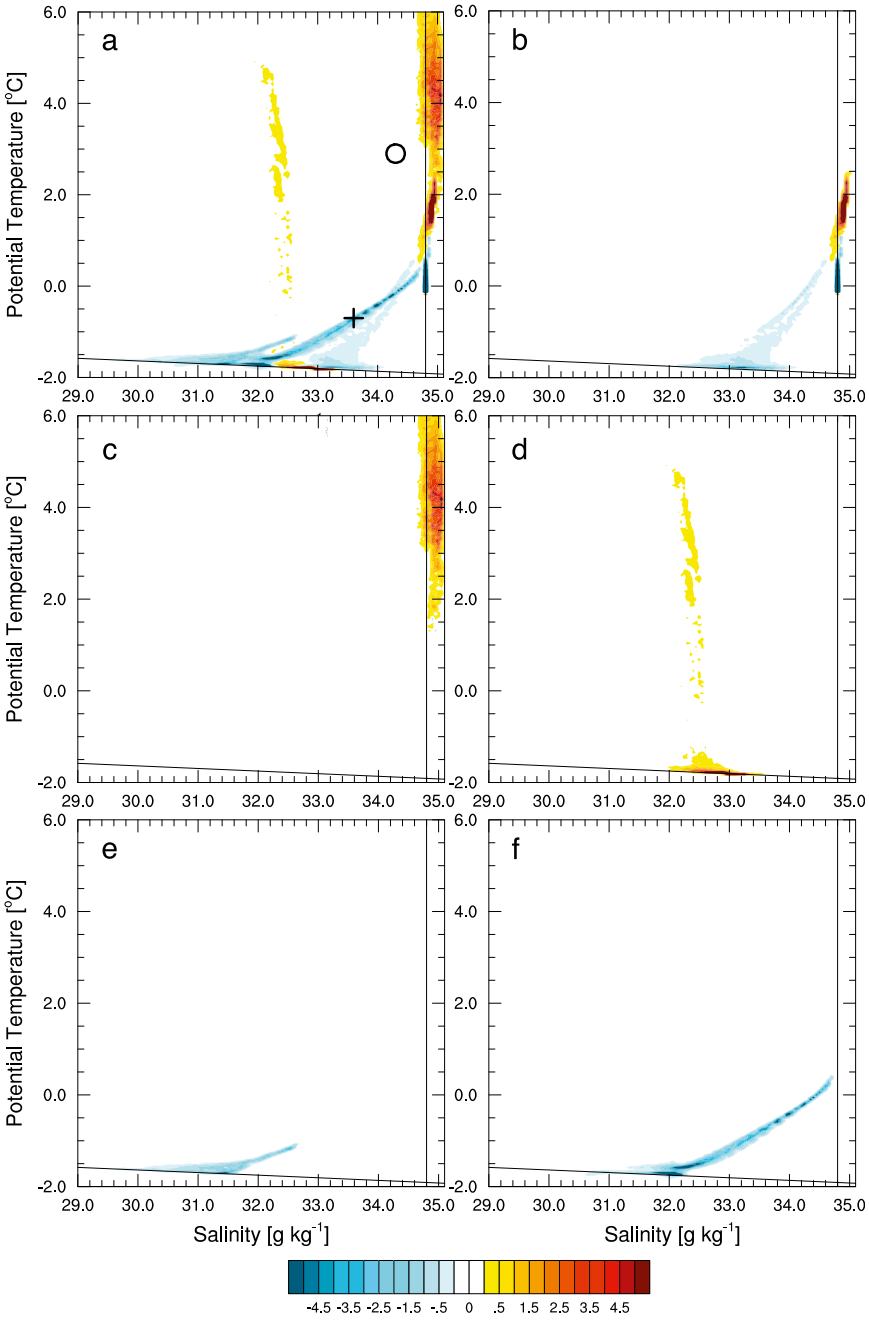

FIG. 11. Net boundary exchange distributions $-m(S, T)$ [10^6 m^3 (s °C S)$^{-1}$] for (a) all gateways, (b) Fram Strait, (c) Barents Sea Opening, (d) Bering Strait, (e) Barrow Strait, and (f) Nares Strait. Note that a positive value (red colors) means a net inflow to the Arctic region. In (a), the transport-weighted mean inflow (circle) and outflow (cross) S–T coordinates are also shown.

f. Arctic Ocean water mass transformations in S–T

Here, we present the Arctic Ocean water mass transformation in S–T coordinates given by the transformation vector $\mathbf{J}$, which is defined in Eq. (5). Using Eqs. (3) and (4), $\mathbf{J}$ can be expressed as

$$\mathbf{J} = \left(S\frac{\partial^2 E}{\partial T \partial S} - \frac{\partial^2 F_S}{\partial T \partial S}, -\frac{1}{c}\frac{\partial^2 Q}{\partial T \partial S} - \frac{1}{c}\frac{\partial^2 F_T}{\partial T \partial S} \right), \quad (16)$$

which shows that the water mass transformations occur as a result of both surface and interior processes.

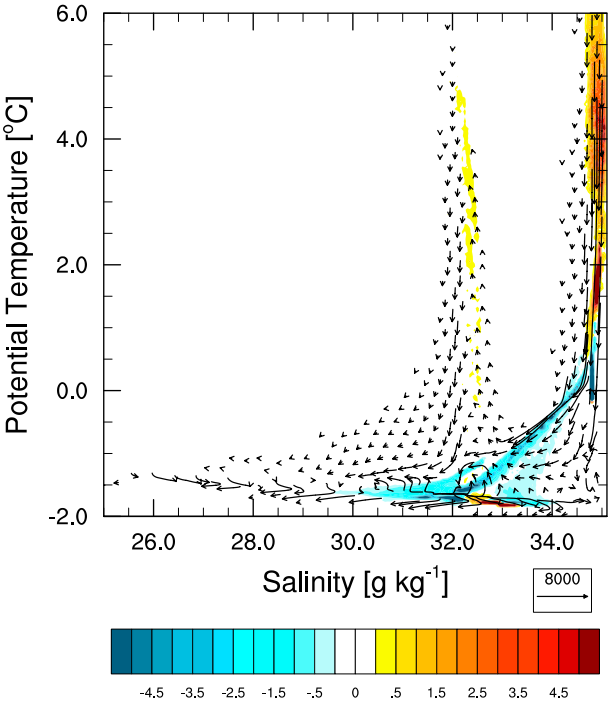

FIG. 12. The total transformation vector **J** and the boundary exchange distributions $-m(S, T)$ [10^6 m^3 (s °C S)$^{-1}$] for the Arctic Ocean.

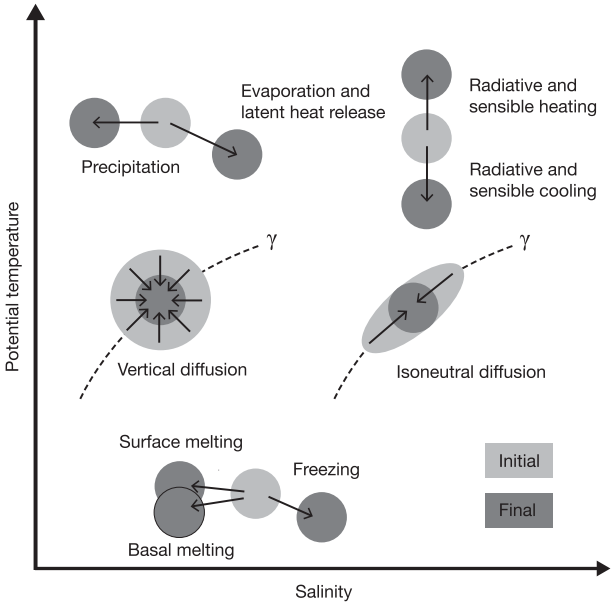

FIG. 13. Schematic based on Groeskamp et al. (2014a) showing how different surface and internal processes act to transform a water parcel in S–T coordinates. Note that the description of the processes is based on how they are formulated in the model and that γ are neutral density lines.

Figure 12 shows **J**, the water mass transformation vector[2] field in the Arctic Ocean and the boundary exchange distribution $m(S, T)$ from our model simulation. The most notable features are the strong cooling of both Atlantic and Pacific water as well as the general freshening of the most abundant water masses (see also Fig. 14a). It is also clearly seen how **J** mostly connects the inflowing water masses with the outflowing water masses, showing the major water mass transformation occurring in the simulated Arctic Ocean. In the colder region, close to the freezing line, where most of the polar mixed layer resides, the transformations are more complex. Here, the slightly warmer water mass is cooled and salinified, whereas just on the freezing line there is mostly a freshening and a slight cooling.

A water parcel can undergo a transformation in S–T space because of a number of different surface and interior processes, summarized in Fig. 13. To study how the different processes contribute to the total transformation we decompose **J**, in a similar manner as section 3d, into its most important components as $\mathbf{J}_{tot} \approx \mathbf{J}_{sur} + \mathbf{J}_{vert} + \mathbf{J}_{iso}$, representing surface processes, vertical mixing, and isoneutral mixing. Note that we have also examined all other processes in the model that contribute to the explicit diffusive and surface fluxes such as convection and the bottom boundary layer parameterization. They were, however, found to be of much less importance for the total transformation in this model.

Figure 14 shows the transformation vector decomposed into its major components. An immediate question is what processes transform the generally warm and saline inflow waters to the cold and fresher outflow waters (see Fig. 11). In this perspective, the most striking feature of the transformations, at least in the S–T regions away from the freezing line, is that the surface processes primarily transform the Arctic Ocean water masses in the T direction toward colder temperatures and that the vertical mixing transforms in the S direction toward lower salinity. The reason is that the significant transformation toward lower salinity occurs in a S–T range that occupies a small surface area fraction of the Arctic Ocean (see Fig. 6). Thus, these water masses are only to a small degree directly influenced by the surface freshwater flux. Close to the freezing line, the surface processes act to either cool and salinify or cool and freshen the water mass. Here, the transformation is generally directed away from the narrow

[2] Note that a transformation vector **J** plotted in Figs. 12, 14, and 15 represents the magnitude and direction of the water transformation from the starting point of the vector; however, the end point of the arrow is not the end point of the transformation.

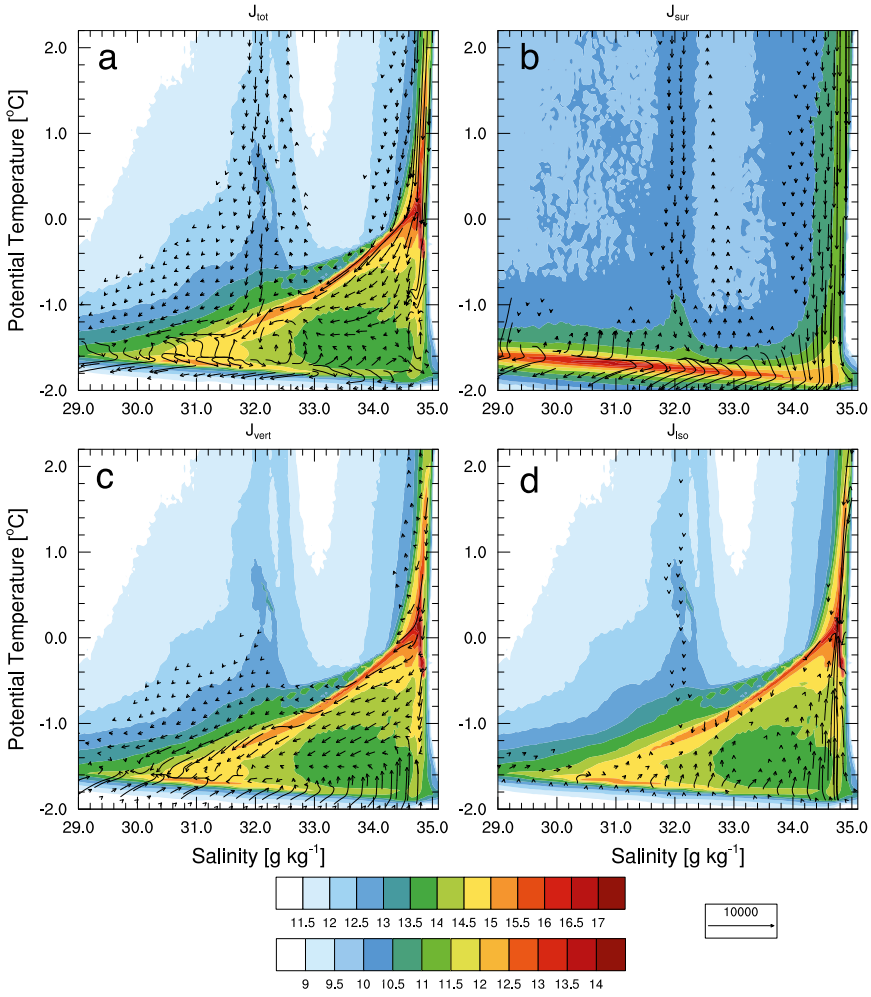

FIG. 14. The process-by-process decomposition of the time-mean transformation vector **J** showing (a) the total transformation, (b) surface processes, (c) vertical mixing, and (d) isoneutral mixing. For (a),(c), and (d), the vectors are plotted on top of the time-mean $v(S, T)$ $\{\log10\ [m^3\ (°C\ S)^{-1}]\}$, while (b) is plotted on top of the $a(S, T)$. The upper color bar is for the $v(S, T)$, and the lower color bar is for the $a(S, T)$ distributions.

band of temperature–salinity classes that occupy the largest area at the sea surface. Thus, the surface fluxes strive to broaden the S–T distribution at the surface. This is partly balanced by the vertical mixing, which strives to warm and salinify the cold and freshwater. It is also seen that the isoneutral mixing has a less important role for most parts of the Arctic Ocean water mass in this model. However, it is important in a narrow salinity range $S \in [34.5, 34.9]\ g\,kg^{-1}$, where it predominantly acts in the T direction to either cool or warm, yielding a transformation directed toward a central water mass with a large volumetric abundance. As the density is mainly determined by salinity in the Arctic Ocean, the neutral density surfaces are roughly aligned with the isohaline surfaces and the isoneutral mixing thus mostly occurs across isothermal surfaces.

To further examine the transformations close to the freezing line, we compute the time-mean transformations for the winter (October–March) and summer (April–September) seasons from our simulation. Figure 15 shows that the net transformation vector $\mathbf{J}_{tot}$ is quite different for the two seasons. During winter, there is a general cooling over the whole S–T plane with a slight freshening in the halocline region and a salinification close to the freezing line. During the summer, most of the S–T domain shows a general warming except near the freezing line and in the model's lower halocline region, close to the Atlantic water core, where there is a cooling and freshening. The process-by-process decomposition shows that it is mainly the surface flux–related $\mathbf{J}_{sur}$ that contributes to the seasonal signal, as could be expected. During

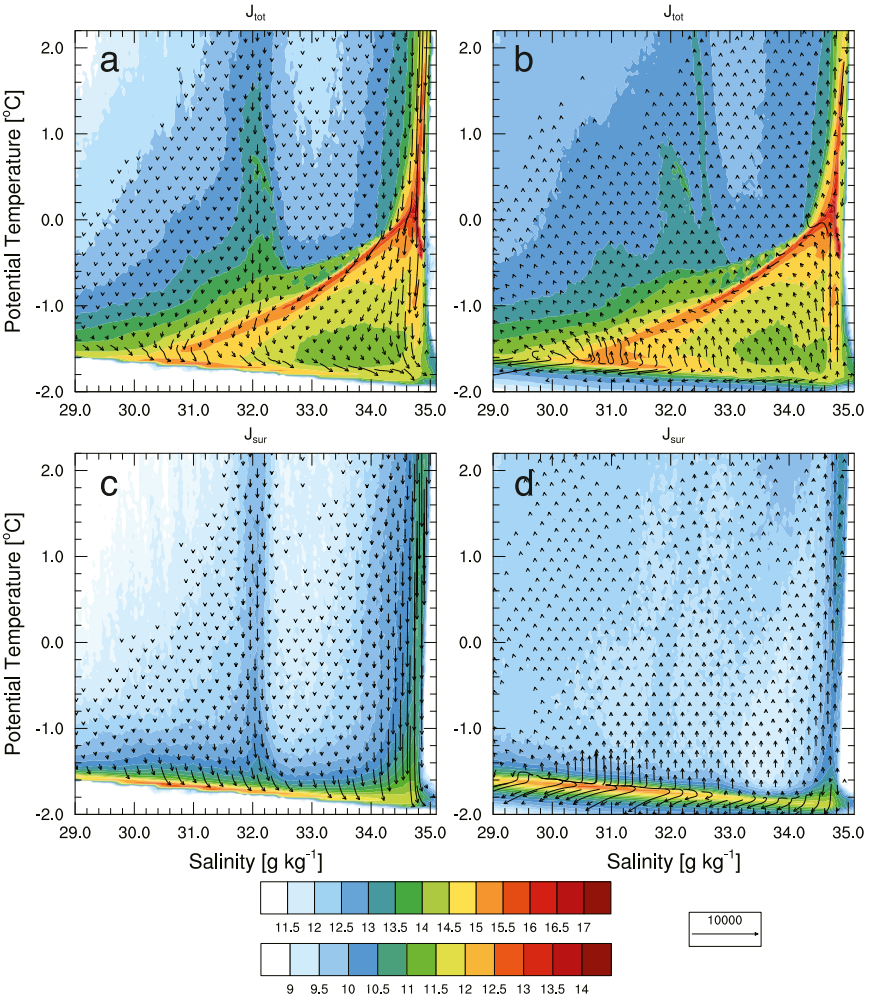

FIG. 15. The process-by-process decomposition of the seasonal time-mean **J** showing (a), (b) the total transformation, (c),(d) surface processes, (e),(f) vertical mixing, and (g),(h) isoneutral mixing. For (a), (b), and (e)–(h), the vectors are plotted on top of the seasonal $v(S, T)$ {log10 [m^3 (°C S)$^{-1}$]}, while (b) and (c) are plotted on top of the seasonal $a(S, T)$. (left) Winter conditions (October–March) and (right) summer conditions (April–September). The upper color bar is for the $v(S, T)$, and the lower color bar is for the $a(S, T)$ distributions.

winter, the surface heat loss and ice formation leads to a transformation toward colder and more saline water masses. During summer, on the other hand, heat gain yields a transformation toward warmer water, except near the freezing line where there is a pronounced freshening and cooling. Presumably, this reflects solar and atmospheric heating of surface water in the sea ice leads and in the marginal ice zone, which results in basal and lateral ice melt. We also find an additional freshening from the sea surface restoration. It can be noted that the slope of the transformation vectors are generally less steep than would be the result if warmer water melted ice without any external input of heat and freshwater (Gade 1979). The summer transformation toward colder water due to the surface fluxes is partly counteracted by the transformation due to mixing. It is also seen that the transformation due to isoneutral mixing has a more moderate seasonal change compared to the vertical mixing.

The divergence of the transformation vector yields the net formation ($\nabla \cdot \mathbf{J} < 0$) or destruction ($\nabla \cdot \mathbf{J} > 0$) of a certain water class. According to Eq. (6) the divergence should balance the net sources and sinks of water from the boundary exchange term $-m(S, T)$ and the freshwater exchange $-e(S, T)$. Assuming that $e(S, T)$ is negligible, we have that $\nabla \cdot \mathbf{J} \approx -m(S, T)$. Figures 16a and 16b show that in the model S–T regions with a net inflow (outflow) generally correspond to

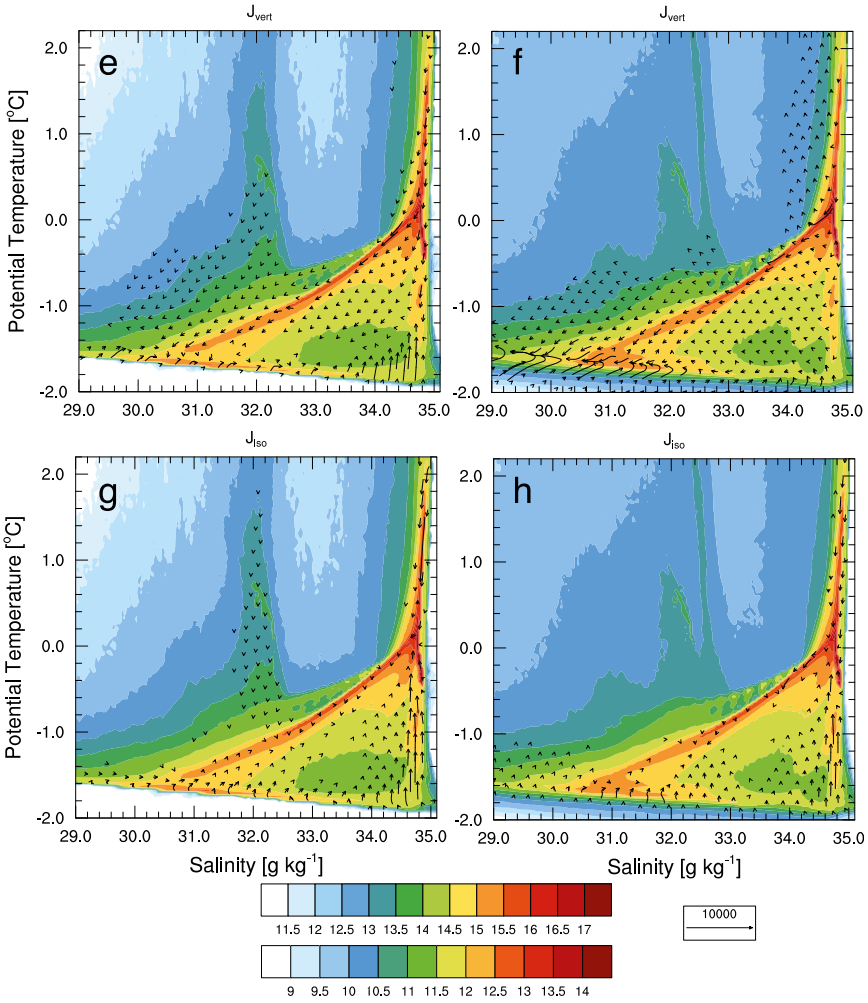

FIG. 15. (*Continued*)

destruction (formation) regions, although the divergence field is rather noisy. Particularly, S–T classes occupying inflowing Atlantic and Pacific water show a destruction of the source waters, and the S–T classes occupying outflowing Polar Surface Water (including the band covering the halocline and lower Atlantic water S–T region) show a formation. Two bands along the freezing line are also seen where there is formation in the slightly colder band and destruction in the warmer band.

To further examine the role of the surface and internal processes, we decompose the divergence as $\nabla \cdot \mathbf{J} = \nabla \cdot \mathbf{J}_{\text{sur}} + \nabla \cdot \mathbf{J}_{\text{int}}$, where $\mathbf{J}_{\text{int}} = \mathbf{J}_{\text{vert}} + \mathbf{J}_{\text{iso}}$. Figures 16c and 16d show that the surface and internal terms generally show opposing sign and partly counteract each other. Water occupying inflowing Atlantic and Pacific water classes are primarily destroyed by the surface processes that are partly balanced by the internal processes. Along the formation/destruction bands following the freezing line, it is seen that the surface processes form the water classes in the slightly colder band, and the internal processes partly oppose this formation, leading to a reduced net formation. In the warmer band, it is the opposite situation. A region not showing the opposing sign between the surface and interior terms is the band covering the halocline and lower Atlantic water S–T region. Here, instead, both surface and internal processes act to form these water classes, with the internal mixing term dominating.

It is also clear that there are regions where there is a divergence that does not balance the $m(S, T)$. Analysis of the neglected $e(S, T)$ term (not shown) does not compensate for this inconsistency. Model drift of the $v(S, T)$ could also have contributed, but in our case it is small. Instead, we assume that the inconsistency is because of the models' linear free-surface treatment, errors induced by sampling and discretization in S–T space, and possibly numerical diffusion.

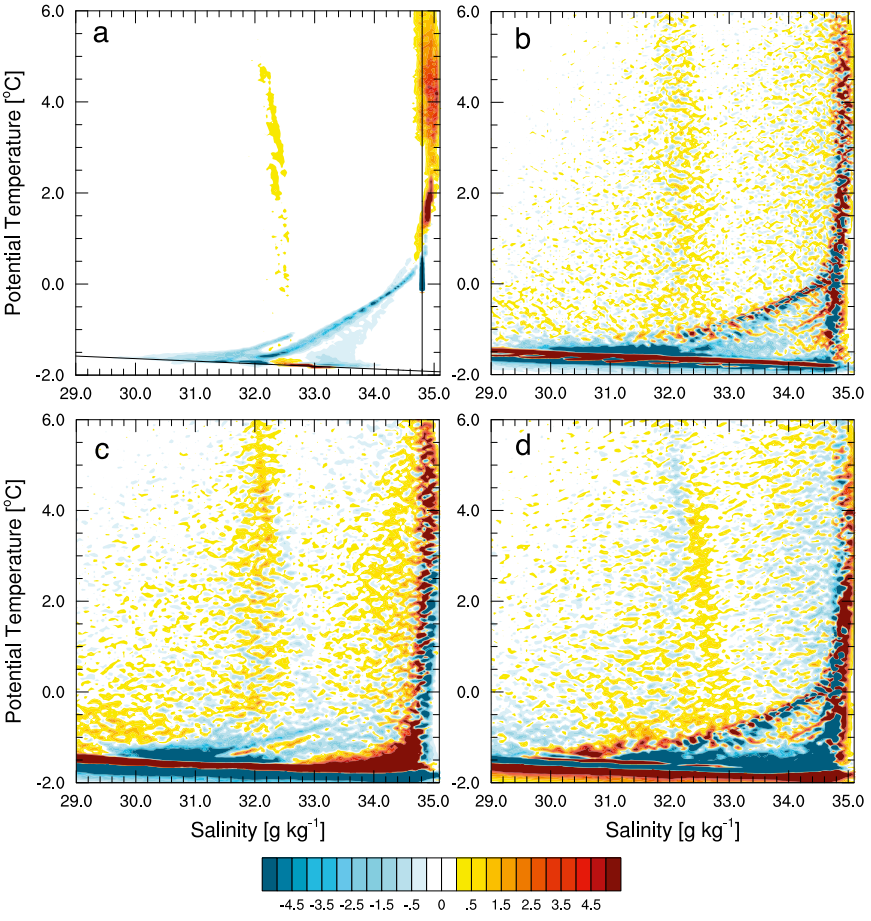

FIG. 16. (a) The time-mean boundary exchange distribution $-m(S, T)$ for all gateways enclosing the Arctic Ocean, (b) the total divergence $\mathbf{V} \cdot \mathbf{J}$, (c) the divergence due to surface processes $\mathbf{V} \cdot \mathbf{J}_{\text{sur}}$, and (d) the divergence due to internal processes $\mathbf{V} \cdot \mathbf{J}_{\text{int}}$ [10^6 m^3 (s °C S)$^{-1}$]. Red colors show water mass destruction and blue colors show formation.

g. *Model deficiencies and water mass transformations in S–T coordinates*

We have analyzed the water mass transformation in the Arctic Ocean using a global ocean circulation model. Because of the model deficiencies, some aspects of the results are idiosyncratic to the model in use and might not be representative of the real ocean. For instance, Figs. 3 and 4 show that the Atlantic water core temperature is too cold and that the cold halocline is not well represented in the model. Holloway et al. (2007) found similar problems when analyzing the Arctic Ocean hydrography in a suite of different models, including both global and regional configurations. Below we briefly discuss how the Walin framework approach may reveal information on which model features and processes cause the differences between the observational and model-simulated hydrographic distribution.

When comparing model simulations and observations, the volume and area distribution functions are useful complements to traditional S–T diagrams. Figure 6 reveals that the model has too much water in a ridgelike S–T band that extends from $S \sim 34.5\,\text{g kg}^{-1}$ and $T \sim 0$°C toward $S \sim 30\,\text{g kg}^{-1}$ and $T \sim -1.8$°C. This water mass is not present in the observations, where the maximum in $\upsilon(S, T)$ in this range is encountered closer to the freezing line, forming a curve-shaped feature for $S \in [31.5, 34.5]\,\text{g kg}^{-1}$. As already noted, the Atlantic water in the model is too cold. To examine the reason for the model biases in hydrography, we consider the inflow and outflow distributions shown in Fig. 11. We note that the S–T distribution of the inflowing waters are in more reasonable agreement with observations than the distribution of the outflowing water masses, which tend to be too warm for the halocline water and too cold for the Atlantic water in the model. Thus, the hydrographic

model bias appears to be primarily produced within the Arctic Ocean.

Figure 14 suggests that vertical mixing between inflowing Atlantic water and colder and fresher surface waters contribute to form the spurious ''too warm'' halocline waters in the model; the vertical mixing causes excessive transformation toward lower salinity. Inspections of the model fields reveal that the Barents Sea branch of the Atlantic inflow is too cold when entering the St. Anna Trough and that there is no cyclonic Arctic boundary current in the Canada basin. In addition, Figs. 9b and 14 show that the isoneutral mixing together with surface heat loss are the major components contributing to a transform toward lower temperatures for Atlantic water, and Fig. 8b shows that isoneutral and vertical mixing dominate transformations toward lower salinities in the Atlantic water salinity range. These features also contribute to the cold bias of the Atlantic water in the model.

The absence of a cold halocline in the model seems thus to be partly related to excessive mixing of heat into the upper ocean. However, another cause could be insufficient sea ice–related formation of near–freezing point water in the model. Aagaard et al. (1981) proposed that the strong wintertime surface heat loss and sea ice formation on the shallow shelves are important processes for creating cold halocline water as well as cold, denser water. Figures 15c and 16b indicate that near–freezing point water is formed during winter in the model. However, Fig. 8b shows that the freshwater flux due to the restoration of the sea surface salinity results in a freshening that counteracts and reduces the salinification associated with sea ice formation for $S \in [31, 34]\,\mathrm{g\,kg^{-1}}$. The counteracting ''restoring'' transformation occurs primarily along the Barents Sea, Kara Sea, Laptev Sea, and Chukchi Sea coasts as well as close to the large Arctic island; these are all regions with strong sea ice formation (not shown). This suggests that the surface salinity restoration in this model, while ''correcting'' surface biases, presumably acts to reduce the formation rate of cold halocline water, thereby causing biases in the subsurface hydrography. Surface salinity restoration may also play a role in the transformation pattern close to the freezing line. As noted earlier, the transformations during the summer season, in Fig. 15, show a strong freshening and a slight cooling. Partly, we assume that this reflects that water slightly warmer than the freezing point induces lateral and basal ice melt in sea ice leads and the marginal ice zone. However, also here the restoring fluxes may contribute to the transformation pattern. At the end of the summer we find that in open-ocean areas the combination of heat loss and restoring flux, which acts to freshen these areas, also gives a freshening and cooling pattern close to the freezing line.

4. Summary and conclusions

In this study, we have investigated water mass transformations in the Arctic Ocean using the S–T Walin framework developed by Hieronymus et al. (2014). The method has been applied to the global general circulation model NEMO, run in the ORCA1 configuration. By diagnosing the surface and internal diffusive fluxes, we have studied the resulting water mass transformations in S–T space. In particular, we have studied how the inflowing waters, encompassing both relatively warm and salty Atlantic water and fresher Pacific water, are transformed within the Arctic Ocean into polar mixed layer and halocline waters, which compose the outflowing water masses. As anticipated, the most dominant water mass transformation is a cooling and freshening of the inflowing waters (e.g., Rudels 2009; Tsubouchi et al. 2012). The calculated water mass transformation vector $\mathbf{J}$ shows how the inflowing waters are transformed to outflowing waters in S–T space.

By decomposing $\mathbf{J}$ into different processes representing the parameterized air–sea and ice–sea surface exchange and interior mixing, we have examined the relative importance of these processes in transforming the inflowing water, shaping both the hydrographic state within the Arctic Ocean [represented by the volumetric distribution function $v(S, T)$ and the area function $a(S, T)$] and the S–T properties of the waters that exit the basin. Our analyses show that for S–T classes away from the freezing line, it is primarily the surface heat loss that transforms the Arctic Ocean water toward colder temperatures, while vertical mixing transforms toward lower salinities. Surface freshwater input is important for transformations occurring for salinities below $30\,\mathrm{g\,kg^{-1}}$, but the resulting net transformation at these low salinities is essentially negligible (see Figs. 7 and 8).

For S–T regions close to the freezing line, the transformations are more complex because of the seasonality of the surface fluxes and the growth/melt of sea ice. During the winter season, the surface fluxes yield a net transformation toward colder temperatures and higher salinity in this S–T region, reflecting sea ice formation and heat loss to the atmosphere. During summer, on the other hand, there is mainly a transformation toward lower salinities and slightly lower temperatures, reflecting ice melt and some surface heat input that reduces the cooling of the surface water. However, for waters that are slightly warmer than the freezing temperature, there is a pronounced transformation toward higher temperatures.

Away from the freezing line, the annual-mean transformation is qualitatively similar to the wintertime transformation. However, for the coldest water below salinities of about $S \sim 32\,\mathrm{g\,kg^{-1}}$, the annual-mean transformation more closely resembles the summertime transformation. This illustrates the importance of the seasonal cycle for the annual-mean water mass transformation.

The Arctic Ocean water transformations show many similarities with those of the global ocean. For instance, the surface fluxes tend to deplete water in the S–T classes that occupy the largest surface area, thereby creating the extremes, whereas the mixing processes act to reduce the temperature and salinity ranges, as was found in the study of global water mass transformations by Hieronymus et al. (2014). However, unlike the global case where in each S–T interval the formation of water masses due to surface fluxes and mixing must exactly cancel each other in a steady state, this is not required in the Arctic Ocean where flows across its boundaries introduce sources and sinks of water masses. Thus, for the Arctic Ocean the net water mass transformation due to surface fluxes and mixing is significant and necessary for connecting the sinks and sources of water masses that are associated with the exchange with the Atlantic and Pacific Oceans.

We believe that the water mass transformations diagnosed from the present ocean circulation model qualitatively capture the broad features of the water mass transformations in the real Arctic Ocean. However, there are model deficiencies in processes that are important for the water mass transformations and the use of sea surface salinity restoring creates spurious transformation. In addition, problems related to salt conservation (partly related to sea ice processes and free-surface treatment) results in an uncomfortably large residual in the S-coordinate salt budget. Accordingly, some of the more detailed features of the water mass transformation in S–T space are unrealistic in the present simulation. However, we argue in section 3g that to compute and analyze the water mass transformation in an ocean circulation model can highlight the performance of parameterized subgrid processes that ultimately cause the transformations.

It is of worth to briefly comment on observationally based application of water mass transformation studies of the Arctic Ocean. Data applications of the Walin formalism have mainly focused on water mass transformations due to air–sea fluxes, for example, Andersson et al. (1982), Tziperman (1986), and Speer (1993). In the Arctic Ocean, the transformations due to air–sea fluxes are difficult to compute because of the limited data, but crude estimates should be obtainable. The observations needed for computing the net inflow as a function of temperature and salinity are presumably better and a few computations have been made for the Fram Strait flow (e.g., Rudels 1987; Nilsson et al. 2008; Rudels et al. 2008) and for all circum-Arctic gateways over a 32-day period (Tsubouchi et al. 2012). Thus, there is some potential for the estimating of the water mass export and the water mass formation due to surface fluxes in S–T coordinates for the Arctic Ocean. Assuming a steady state, this would allow the water mass formation due to interior mixing ($-\nabla \cdot \mathbf{J}_{\mathrm{int}}$) to be diagnosed. Note that this is not enough information for the estimating $\mathbf{J}_{\mathrm{int}}$ itself, as it may also have a nondivergent component. In any event, it is somewhat doubtful that the present Arctic Ocean observations are good enough to make such a computation meaningful. Possibly, the inverse-modeling approach in S–T coordinates developed by Groeskamp et al. (2014b) could be utilized to improve the accuracy of observationally based Arctic Ocean water mass transformation studies.

Acknowledgments. P. Pemberton and H. E. M. Meier were supported by the project Advanced Simulation of Arctic Climate Change and Impact on Northern Regions (ADSIMNOR, 214-2009-389) funded by the Swedish Research Council for Environment, Agricultural Sciences, and Spatial Planning (FORMAS). J. Nilsson acknowledges support from the Knut and Alice Wallenberg Foundation (via the SWERUS-C3 program) and the Swedish National Space Board. The authors would like to thank Jan D. Zika and an anonymous reviewer for comments that helped improve the presentation and content of the manuscript.

APPENDIX A

Definitions

Following Hieronymus et al. (2014), we here consider a region in the ocean bounded by the sea surface, the sea floor, and an interior vertical boundary B (see Fig. 1). To describe the state and evolution of the water properties in the region, we introduce the following variables and flows:

$R(S, T, t)$	Subregion having a salinity less than S and a temperature less than T.
$V(S, T, t)$	Volume of R.
$A(S, T, t)$	The sea surface area, including sea ice–covered regions, where the salinity is less than S and the temperature less than T.
$I_T(S, T, t)$	The part of the isothermal surface T where the salinity is less than S.
$I_S(S, T, t)$	The part of the isohaline surface S where the temperature is less than T.
$G_T(S, T, t)$	The volume flow penetrating the isothermal surface $I_T(S, T, t)$, counted positive when leaving the region.

$G_S(S, T, t)$ Volume flow penetrating the isohaline surface $I_S(S, T, t)$, counted positive when leaving the region.

$M(S, T, t)$ The volume flow having a salinity less than S and a temperature less than T that exits through the interior control surface B.

$E(S, T, t)$ Net volume flow of freshwater exiting across the surface $A(S, T, t)$, that is, evaporation minus precipitation, net ice melt, and runoff from land.

$Q(S, T, t)$ The net sea surface heat flux out of $A(S, T, t)$.

$F_T(S, T, t)$ The diffusive heat flux through the surfaces $I_T(S, T, t)$ and $I_S(S, T, t)$ (and, when used, B), counted positive when leaving the region.

$F_S(S, T, t)$ The diffusive salt flux through the surfaces $I_T(S, T, t)$ and $I_S(S, T, t)$ (and, when used, B), counted positive when leaving the region.

APPENDIX B

Basic Relations

Based on the definitions above, we will now formulate equations describing the conservation of volume, heat, and salt for a region $R(S, T, t)$.

Starting with the conservation of volume, we can express it as follows:

$$\frac{\partial V}{\partial t} = -G_T - G_S - M - E. \tag{B1}$$

Conservation of heat is then given by

$$\begin{aligned} c\frac{\partial}{\partial t}\int_{T_{\min}}^{T} T'\frac{\partial V}{\partial T'}dT' &= -cTG_T - \int_{T_{\min}}^{T} cT'\left(\frac{\partial G_S}{\partial T'} + \frac{\partial M}{\partial T'} + \frac{\partial E}{\partial T'}\right)dT' \\ &\quad - F_T - Q, \end{aligned} \tag{B2}$$

where $T_{\min}$ is the lowest temperature in the domain. The terms on the right-hand side are the advective heat transport across I_T; the advective heat transport across I_S, A, and B; the diffusive flux across I_T and I_S; and the net heat loss across A. Note that the temperature of precipitation and river input are assumed to be equal to the local SST in our heat budget.

Similarly, the conservation of salt can be written as

$$\frac{\partial}{\partial t}\int_0^S S'\frac{\partial V}{\partial S'}dS' = -SG_S - \int_0^S S'\left(\frac{\partial G_T}{\partial S'} + \frac{\partial M}{\partial S'}\right)dS' - F_S. \tag{B3}$$

By differentiating Eqs. (B1) and (B3) with respect to S and then multiplying the first with S and subtracting it from the latter one obtains

$$G_S = S\left(\frac{\partial E}{\partial S}\right) - \frac{\partial F_S}{\partial S}. \tag{B4}$$

This equation expresses that water with salinity S leaving the region R by crossing I_S must become more saline, which is accomplished by surface processes (the first term) and interior diffusion (the second term). Similarly, manipulating Eqs. (B1) and (B2) yields

$$G_T = -\frac{1}{c}\frac{\partial Q}{\partial T} - \frac{1}{c}\frac{\partial F_T}{\partial T}. \tag{B5}$$

This expresses that water with temperature T leaving R across I_T does so as a result of heating by surface fluxes and interior diffusion.

APPENDIX C

Salinity- or Temperature-Only Coordinates (Walin's 1D Frameworks)

The equations above are related to the 1D frameworks by Walin (1977, 1982), and we will now describe how they are recovered from the S–T framework. The salinity-only coordinate case of Walin (1977) can be recovered by letting $T = T_{\max}$ in Eqs. (B1) and (B3), where $T_{\max}$ is the largest temperature in the domain.

In the salinity-only coordinate case, the continuity equation for the volume in the ocean where the salinity is less than S is then given by

$$\begin{aligned} \frac{\partial V(S, T_{\max}, t)}{\partial t} &= -G_S(S, T_{\max}, t) - M(S, T_{\max}, t) \\ &\quad - E(S, T_{\max}, t), \end{aligned} \tag{C1}$$

with $G_S(S, T_{\max}, t)$ being the volume transport across the entire isohaline surface S. By using the salt conservation of Eq. (B3) and assuming a steady state, that is, $G_S(S, T_{\max}) + E(S, T_{\max}) + M(S, T_{\max}) = 0$, the salt balance can be formulated as

$$F_S(S, T_{\max}) = SE(S, T_{\max}) + \int_0^S M(S', T_{\max})\,dS'. \tag{C2}$$

Equation (C2) shows that in a steady state, the diffusive salt flux across the isohaline S is balancing the virtual salt flux $SE(S, T_{\max})$ and the boundary salt flux $\int_0^S M(S', T_{\max})\, dS'$ across the surface B where salinity is less than S.

Likewise, the temperature-only coordinate case of Walin (1982) can be recovered by letting $S = S_{\max}$ in Eq. (B1), where $S_{\max}$ is the largest salinity in the domain. This leads to the continuity equations for temperatures less than T:

$$\frac{\partial V(S_{\max}, T, t)}{\partial t} = -G_T(S_{\max}, T) - M(S_{\max}, T, t) - E(S_{\max}, T, t). \tag{C3}$$

By using the heat conservation Eq. (B2) and assuming a steady state such that $G_T(S_{\max}, T) + E(S_{\max}, T) + M(S_{\max}, T) = 0$, the heat balance for the part of the ocean where the temperature is less than T consequently takes the form

$$F_T(S_{\max}, T) = -Q(S_{\max}, T) + c\int_{T_{\min}}^{T} E(S_{\max}, T')\, dT' + c\int_{T_{\min}}^{T} M(S_{\max}, T')\, dT'. \tag{C4}$$

Here, the diffusive heat flux across the isothermal surface T is balancing the net surface heat loss over the part of the ocean surface where the temperature is less than T and the boundary heat flux $c\int_{T_{\min}}^{T} M(S_{\max}, T')\, dT'$ across B where the temperature is less than T. Note that the integral over $E(S_{\max}, T)$ represents the contribution to the surface heat flux due to the heat transfer associated with the net freshwater exchange.

REFERENCES

Aagaard, K., L. K. Coachman, and E. C. Carmack, 1981: On the halocline of the Arctic Ocean. *Deep-Sea Res.,* **28A,** 529–545, doi:10.1016/0198-0149(81)90115-1.

Aksenov, Y., S. Bacon, A. C. Coward, and N. P. Holliday, 2010: Polar outflow from the Arctic Ocean: A high resolution model study. *J. Mar. Syst.,* **83,** 14–37, doi:10.1016/j.jmarsys.2010.06.007.

Andersson, L., B. Rudels, and G. Walin, 1982: Computations of heat flux through the ocean surface as a function of temperature. *Tellus,* **34,** 196–198, doi:10.1111/j.2153-3490.1982.tb01807.x.

Beckmann, A., and R. Döscher, 1997: A method for improved representation of dense water spreading over topography in geopotential-coordinate models. *J. Phys. Oceanogr.,* **27,** 581–591, doi:10.1175/1520-0485(1997)027<0581:AMFIRO>2.0.CO;2.

Beszczynska-Möller, A., E. Fahrbach, U. Schauer, and E. Hansen, 2012: Variability in Atlantic water temperature and transport at the entrance to the Arctic Ocean, 1997–2010. *ICES J. Mar. Sci.,* **69,** 852–863, doi:10.1093/icesjms/fss056.

Brambilla, E., L. D. Talley, and P. E. Robbins, 2008: Subpolar Mode Water in the northeastern Atlantic: 2. Origin and transformation. *J. Geophys. Res.,* **113,** C04026, doi:10.1029/2006JC004063.

Brodeau, L., B. Barnier, A.-M. Treguier, T. Penduff, and S. Gulev, 2010: An ERA40-based atmospheric forcing for global ocean circulation models. *Ocean Modell.,* **31,** 88–104, doi:10.1016/j.ocemod.2009.10.005.

Carmack, E. C., 2007: The alpha/beta ocean distinction: A perspective on freshwater fluxes, convection, nutrients and productivity in high-latitude seas. *Deep-Sea Res. II,* **54,** 2578–2598, doi:10.1016/j.dsr2.2007.08.018.

de Steur, L., E. Hansen, R. Gerdes, M. J. Karcher, E. Fahrbach, and J. Holfort, 2009: Freshwater fluxes in the East Greenland Current: A decade of observations. *Geophys. Res. Lett.,* **36,** L23611, doi:10.1029/2009GL041278.

Döös, K., J. Nilsson, J. Nycander, L. Brodeau, and M. Ballarotta, 2012: The World Ocean thermohaline circulation. *J. Phys. Oceanogr.,* **42,** 1445–1460, doi:10.1175/JPO-D-11-0163.1.

Eldevik, T., and J. E. Ø. Nilsen, 2013: The Arctic–Atlantic thermohaline circulation. *J. Climate,* **26,** 8698–8705, doi:10.1175/JCLI-D-13-00305.1.

Emile-Geay, J., and G. Madec, 2008: Geothermal heating, diapycnal mixing and the abyssal circulation. *Ocean Sci. Discuss.,* **5,** 281–325, doi:10.5194/osd-5-281-2008.

Fichefet, T., and M. A. Maqueda, 1997: Sensitivity of a global sea ice model to the treatment of ice thermodynamics and dynamics. *J. Geophys. Res.,* **102,** 12 609–12 646, doi:10.1029/97JC00480.

Gade, H. G., 1979: Melting of ice in sea water: A primitive model with application to the Antarctic ice shelf and icebergs. *J. Phys. Oceanogr.,* **9,** 189–198, doi:10.1175/1520-0485(1979)009<0189:MOIISW>2.0.CO;2.

Gaspar, P., Y. Grégoris, and J.-M. Lefevre, 1990: A simple eddy kinetic energy model for simulations of the oceanic vertical mixing: Tests at Station Papa and long-term upper ocean study site. *J. Geophys. Res.,* **95,** 16 179–16 193, doi:10.1029/JC095iC09p16179.

Gent, P. R., and J. C. McWilliams, 1990: Isopycnal mixing in ocean circulation models. *J. Phys. Oceanogr.,* **20,** 150–155, doi:10.1175/1520-0485(1990)020<0150:IMIOCM>2.0.CO;2.

Groeskamp, S., J. D. Zika, T. J. McDougall, B. M. Sloyan, and F. Laliberté, 2014a: The representation of ocean circulation and variability in thermodynamic coordinates. *J. Phys. Oceanogr.,* **44,** 1735–1750, doi:10.1175/JPO-D-13-0213.1.

——, ——, B. M. Sloyan, T. J. McDougall, and P. C. McIntosh, 2014b: A thermohaline inverse method for estimating diathermohaline circulation and mixing. *J. Phys. Oceanogr.,* **44,** 2681–2697, doi:10.1175/JPO-D-14-0039.1.

Hieronymus, M., J. Nilsson, and J. Nycander, 2014: Water mass transformation in salinity–temperature space. *J. Phys. Oceanogr.,* **44,** 2547–2568, doi:10.1175/JPO-D-13-0257.1.

Holloway, G., and Coauthors, 2007: Water properties and circulation in Arctic Ocean models. *J. Geophys. Res.,* **112,** C04S03, doi:10.1029/2006JC003642.

Iudicone, D., G. Madec, and T. J. McDougall, 2008: Water-mass transformations in a neutral density framework and the key role of light penetration. *J. Phys. Oceanogr.,* **38,** 1357–1376, doi:10.1175/2007JPO3464.1.

Madec, G., 2008: NEMO ocean engine. Institut Pierre-Simon Laplace Note du Pole de modélisation 27, 367 pp. [Available online at www.nemo-ocean.eu/About-NEMO/Reference-manuals.]

——, P. Delecluse, M. Imbard, and C. Levy, 1998: OPA 8.1 ocean general circulation model reference manual. Institut Pierre-Simon Laplace Note du Pole de modélisation 11, 97 pp. [Available online at www.nemo-ocean.eu/Media/Files/Doc_OPA8.1.]

Marsh, R., S. A. Josey, A. De Nurser, B. A. Cuevas, and A. C. Coward, 2005: Water mass transformation in the North Atlantic over 1985-2002 simulated in an eddy-permitting model. *Ocean Sci.,* **1,** 127–144, doi:10.5194/os-1-127-2005.

Marshall, D., 1997: Subduction of water masses in an eddying ocean. *J. Mar. Res.,* **55,** 201–222, doi:10.1357/0022240973224373.

Marshall, J., D. Jamous, and J. Nilsson, 1999: Reconciling thermodynamic and dynamic methods of computation of water-mass transformation rates. *Deep-Sea Res. I,* **46,** 545–572, doi:10.1016/S0967-0637(98)00082-X.

Martinson, D. G., and M. Steele, 2001: Future of the Arctic sea ice cover: Implications of an Antarctic analog. *Geophys. Res. Lett.,* **28,** 307–310, doi:10.1029/2000GL011549.

Maze, G., G. Forget, M. Buckley, J. Marshall, and I. Cerovecki, 2009: Using transformation and formation maps to study the role of air–sea heat fluxes in North Atlantic Eighteen Degree Water formation. *J. Phys. Oceanogr.,* **39,** 1818–1835, doi:10.1175/2009JPO3985.1.

Melling, H., and Coauthors, 2008: Fresh-water fluxes via Pacific and Arctic outflows across the Canadian polar shelf. *Arctic–Subarctic Ocean Fluxes,* R. R. Dickson, J. Meincke, and P. Rhines, Eds., Springer, 193–247.

Münchow, A., and H. Melling, 2008: Ocean current observations from Nares Strait to the west of Greenland: Interannual to tidal variability and forcing. *J. Mar. Res.,* **66,** 801–833, doi:10.1357/002224008788064612.

——, K. K. Falkner, and H. Melling, 2007: Spatial continuity of measured seawater and tracer fluxes through Nares Strait, a dynamically wide channel bordering the Canadian Archipelago. *J. Mar. Res.,* **65,** 759–788, doi:10.1357/002224007784219048.

Nilsson, J., 1996: Mixing in the ocean produced by tropical cyclones. *Tellus,* **48A,** 342–355, doi:10.1034/j.1600-0870.1996.t01-1-00010.x.

——, G. Björk, B. Rudels, P. Winsor, and D. J. Torres, 2008: Liquid freshwater transport and Polar Surface Water characteristics in the East Greenland Current during the AO-02 Oden expedition. *Prog. Oceanogr.,* **78,** 45–57, doi:10.1016/j.pocean.2007.06.002.

Paulson, C. A., and J. J. Simpson, 1977: Irradiance measurements in the upper ocean. *J. Phys. Oceanogr.,* **7,** 952–956, doi:10.1175/1520-0485(1977)007<0952:IMITUO>2.0.CO;2.

Pemberton, P., J. Nilsson, and H. E. Markus Meier, 2014: Arctic Ocean freshwater composition, pathways and transformations from a passive tracer simulation. *Tellus,* **66A,** 23988, doi:10.3402/tellusa.v66.23988.

Prinsenberg, S., J. Hamilton, I. Peterson, and R. Pettipas, 2009: Observing and interpreting the seasonal variability of the oceanographic fluxes passing through Lancaster Sound of the Canadian Arctic Archipelago. *Influence of Climate Change on the Changing Arctic and Sub-Arctic Conditions,* J. C. J. Nihoul and A. G. Kostianoy, Eds., Springer, 125–143.

Redi, M. H., 1982: Oceanic isopycnal mixing by coordinate rotation. *J. Phys. Oceanogr.,* **12,** 1154–1158, doi:10.1175/1520-0485(1982)012<1154:OIMBCR>2.0.CO;2.

Roullet, G., and G. Madec, 2000: Salt conservation, free surface, and varying levels: A new formulation for ocean general circulation models. *J. Geophys. Res.,* **105,** 23 927–23 942, doi:10.1029/2000JC900089.

Rudels, B., 1987: On the mass balance of the Polar Ocean, with special emphasis on the Fram Strait. *Nor. Polarinst. Skr.,* **188,** 1–57.

——, 1989: The formation of Polar Surface Water, the ice export and the exchanges through the Fram Strait. *Prog. Oceanogr.,* **22,** 205–248, doi:10.1016/0079-6611(89)90013-X.

——, 2009: Arctic Ocean circulation. *Encyclopedia of Ocean Science,* 2nd ed. J. H. Steele, Ed., Academic Press, 211–225.

——, 2010: Constraints on exchanges in the Arctic Mediterranean—Do they exist and can they be of use? *Tellus,* **62A,** 109–122, doi:10.1111/j.1600-0870.2009.00425.x.

——, L. G. Anderson, and E. Jones, 1996: Formation and evolution of the surface mixed layer and halocline of the Arctic Ocean. *J. Geophys. Res.,* **101,** 8807–8821, doi:10.1029/96JC00143.

——, E. P. Jones, U. Schauer, and P. Eriksson, 2004: Atlantic sources of the Arctic Ocean surface and halocline waters. *Polar Res.,* **23,** 181–208, doi:10.1111/j.1751-8369.2004.tb00007.x.

——, M. Marnela, and P. Eriksson, 2008: Constraints on estimating mass, heat and freshwater transports in the Arctic Ocean: An exercise. *Arctic–Subarctic Ocean Fluxes,* R. R. Dickson, J. Meincke, and P. Rhines, Eds., Springer, 315–341.

Schauer, U., A. Beszczynska-Möller, W. Walczowski, E. Fahrbach, J. Piechura, and E. Hansen, 2008: Variation of measured heat flow through the Fram Strait between 1997 and 2006. *Arctic–Subarctic Ocean Fluxes,* R. R. Dickson, J. Meincke, and P. Rhines, Eds., Springer, 65–85.

Simmons, H. L., S. R. Jayne, L. C. S. Laurent, and A. J. Weaver, 2004: Tidally driven mixing in a numerical model of the ocean general circulation. *Ocean Modell.,* **6,** 245–263, doi:10.1016/S1463-5003(03)00011-8.

Smedsrud, L. H., R. Ingvaldsen, J. E. Ø. Nilsen, and O. Skagseth, 2010: Heat in the Barents Sea: Transport, storage, and surface fluxes. *Ocean Sci.,* **6,** 219–234, doi:10.5194/os-6-219-2010.

Speer, K. G., 1993: Conversion among North Atlantic surface water types. *Tellus,* **45A,** 72–79, doi:10.1034/j.1600-0870.1993.00006.x.

——, and E. Tziperman, 1992: Rates of water mass formation in the North Atlantic Ocean. *J. Phys. Oceanogr.,* **22,** 93–104, doi:10.1175/1520-0485(1992)022<0093:ROWMFI>2.0.CO;2.

Steele, M., J. H. Morison, and T. B. Curtin, 1995: Halocline water formation in the Barents Sea. *J. Geophys. Res.,* **100,** 881–894, doi:10.1029/94JC02310.

——, and Coauthors, 2001: Adrift in the Beaufort Gyre: A model intercomparison. *Geophys. Res. Lett.,* **28,** 2935–2938, doi:10.1029/2001GL012845.

Stigebrandt, A., 1985: On the hydrographic and ice conditions in the northern North Atlantic during different phases of a glaciation cycle. *Palaeogeogr. Palaeoclimatol. Palaeoecol.,* **50,** 303–321, doi:10.1016/0031-0182(85)90074-4.

Tartinville, B., J.-M. Campin, T. Fichefet, and H. Goosse, 2001: Realistic representation of the surface freshwater flux in an ice–ocean general circulation model. *Ocean Modell.,* **3,** 95–108, doi:10.1016/S1463-5003(01)00003-8.

Tsubouchi, T., and Coauthors, 2012: The Arctic Ocean in summer: A quasi-synoptic inverse estimate of boundary fluxes and water mass transformation. *J. Geophys. Res.,* **117,** C01024, doi:10.1029/2011JC007174.

Tziperman, E., 1986: On the role of interior mixing and air–sea fluxes in determining the stratification and circulation of the oceans. *J. Phys. Oceanogr.,* **16,** 680–693, doi:10.1175/1520-0485(1986)016<0680:OTROIM>2.0.CO;2.

Walin, G., 1977: A theoretical framework for the description of estuaries. *Tellus,* **29,** 128–136, doi:10.1111/j.2153-3490.1977.tb00716.x.

——, 1982: On the relation between sea-surface heat flow and thermal circulation in the ocean. *Tellus,* **34,** 187–195, doi:10.1111/j.2153-3490.1982.tb01806.x.

Woodgate, R. A., K. Aagaard, and T. J. Weingartner, 2005: Monthly temperature, salinity, and transport variability of the Bering Strait through flow. *Geophys. Res. Lett.,* **32,** L04601, doi:10.1029/2004GL021880.

Worthington, L. V., 1981: The water masses of the world ocean: some results of a fine-scale census. *Evolution of Physical Oceanography,* C. Wunsch and B. A. Warren, Eds., MIT Press, 42–69.

Zika, J. D., M. H. England, and W. P. Sijp, 2012: The ocean circulation in thermohaline coordinates. *J. Phys. Oceanogr.,* **42,** 708–724, doi:10.1175/JPO-D-11-0139.1.

——, W. P. Sijp, and M. H. England, 2013: Vertical heat transport by ocean circulation and the role of mechanical and haline forcing. *J. Phys. Oceanogr.,* **43,** 2095–2112, doi:10.1175/JPO-D-12-0179.1.